Vascular network modeling for investigation of blood pressure

Author:

Anna Schrøder Lassen

Student ID: fhr956 (KU)/ s173461 (DTU)

Main supervisor:

Jens Christian Brings Jacobsen (Biomedicinsk Institut, KU)

DTU supervisor:

Mikael Lenz Strube (Institut for Bioteknologi og Biomedicin, DTU)

Bachelor project (20 ECTS)

Biomedicinsk Institut

University of Copenhagen

10 June 2020

Contents

Abstract

Across species, mammals tend to have a mean arterial pressure (MAP) of about 100 mmHg despite variations in mass, activity level and physical proportions. Many studies have hypothesized, investigated and explored possible reasons for the magnitude of this pressure, yet no agreement has seemingly been settled upon. Some studies have found that the differences in MAP between e.g. reptiles, mammals and birds correlate with metabolism rates. In this project, it is therefore hypothesized that the magnitude of MAP is related to an optimal perfusion of the tissues when the energy cost of maintaining blood flow and the volume of the microvasculature is taken into account. To investigate this hypothesis, a computational model of the perfusion of a local microvasculature was created. The model simulates a microvascular bifurcating network, where flow through capillaries is regulated by two mechanisms: 1) Conducted vascular responses initiated from the tissues as a response to tissue oxygenation, and 2) wall shear stress responses. The model was tested for a range of inlet pressures causing adaptations in radii of the internal lumens of the network vessels for two metabolism states. It was found that when the total energy cost of maintaining blood flow and a hypothesized cost of network volume was calculated, a narrow range of possible inlet pressures resulted in a minimum total energy for each metabolism state. The model was furthermore discussed with regards to theoretical perspectives on model elements and to the comparability of results to previous findings and theory. In conclusion, the hypothesis of a mammal MAP of about 100 mmHg as an energy cost optimum related to tissue perfusion was not rejected, and suggestions are also to improve the elements of the computational model which could validate the results further.

Abbreviations

CVR	conducted vascular response
EC	endothelial cell
E-cost	evolutionary cost
G_{ECEC}	EC-EC coupling conductance
MAP	mean arterial pressure
PO_2	partial pressure of oxygen
P_{in}	inlet pressure
P_{out}	outlet pressure
PV-cost	pressure-volume cost (pressure-volume work)
SMC	smooth muscle cell
SO_2	oxygen saturation
SS	shear stress
V_m	membrane potential
$V_{m,rest}$	resting membrane potential
WI	work intensity

Acknowledgements

Thanks to Madeleine Durieux Rostrup-Nielsen for answering many questions about physics.

1 Introduction

Mean arterial pressure (MAP) is a measure of a mean blood pressure in the cardiac cycle, weighted between the systolic and diastolic pressures [1]. Across species, the MAP of mammals tends to center around 100 mmHg [2], differing from for example birds and reptiles. These animals generally have higher and lower arterial pressures than mammals (130 mmHg and 30 mmHg, respectively) [3]. Previous studies have among other things investigated scalings of arterial pressure to body mass [4], the correlation between MAP and the vertical distance between heart and brain [5, 6] and the relation between MAP and vascular flow reserve [7], but no overall agreement about the underlying reason for the above mentioned interval of MAP seems to have been agreed upon. In one study, the authors find correlations between metabolism and MAP: Seymour et al. [3] illustrate a positive correlation between standard metabolic rate and systemic arterial blood pressure based on reptiles, fish, amphibians, mammals and birds. It is therefore possible to imagine that the magnitude of MAP in mammals can be related to an optimal perfusion of the tissues based on tissue metabolism, and that is the focus of this project.

Several methodological approaches have been attempted to investigate the issue of mammal MAP, and some are exemplified by the studies mentioned above: Seymour and Blaylock [2] and Poulsen et al. [4] base their calculations on data from literature search, Sandal et al. [6] base their analysis on data on physical properties as well, Seymour et al. [3] evaluate anatomical evidence, White and Seymour [5] test mathematical models on data on body mass and blood pressure, and Poulsen et al. [7] investigate the issue with a computational model of a microvascular network. When investigating the regulation of blood flow, which involves the complex interaction between various mechanisms, a central challenge lies in exploring the co-operations of these mechanisms. The use of theoretical models, where different biological mechanisms can be united mathematically and computationally is a possible method of solving this problem. Flow regulation in the microcirculation is one example of an area where this is applicable [8].

The purpose of this project is two-fold: First of all (1), the aim is to create a theoretical self-regulatory computational model of a microvascular network, where levels of metabolism in the tissues regulate the blood vessel diameters in order to regulate the blood flow and obtain a sufficient perfusion of tissue. This model is to be used for the second aim (2): To answer the hypothesis that the general magnitude of the mammal MAP (100 mmHg) could be the result of a minimum energy cost for the organism. This energy cost is hypothesized to consist of two elements: First, the energy loss of driving blood through a microvascular network, and second, a hypothetical cost of an increased network volume.

The first type of energy cost corresponds to the energy loss caused by resistance in the microvasculature [9] as a type of pressure-volume work (and will be referred to as the PV-cost). The second cost, however, is based on the idea that a vascular network takes up space in the organism it supplies. The larger the vascular network is, the more space is taken up, leaving less space for the parenchyma. The

underlying assumption for this project is therefore that when a vascular network takes up a larger volume of space, this comes with a price in the form of an energy cost. This cost is assumed to be the product of an evolutionary development and will henceforth be referred to as the E-cost.

Theoretical foundation

In the following sections, the biological theory that lays the ground for above mentioned model and research question is presented. This includes a brief description of the anatomical structure of the vascular network, the transport to, delivery and consumption of oxygen in the tissues, flow regulating mechanisms and calculation of energy cost. In general, this section covers the overall theory and general understanding of the biology that is modelled. Due to the close connection between theory and model in the modelling process, some details and specific relations will be included in the methods section.

1.1 Anatomy of the vascular system

When referring of metabolism in this project, the focus is on the consumption of oxygen, which is a critical component of aerobic metabolism. Oxygen is transported from the lungs and to the tissues of the body via the blood. The pulmonary circulation between heart and lungs ensures oxygenation of the blood, while the systemic circulation between the heart and to the rest of the body ensures the delivery of oxygen to the distant tissues of the body. Blood is transported from the heart through increasingly more narrow arteries, then through the arterioles, precapillary arterioles, capillaries, postcapillary venules, venules, and then the increasingly wider veins. The lumens of veins generally have larger diameters than those of arteries, which decreases the resistance to the lowered blood flow [9]. The part of the system containing vessels with diameters smaller than 100 μm can be categorized as the microcirculation [10]. In the microcirculation, oxygen is exchanged from the blood and to the tissues through networks of capillaries, which are microscopic vessels with semipermeable walls that gases and nutrients can pass through [9]. Capillaries generally have a diameter of 5-10 μm, allowing red blood cells (with a diameter of 7-8 μm) to pass through them [9].

Both arteries and veins have three tissue layers; tunica intima, tunica media and tunica externa, of which the two first contain elements relevant for this project: First of all, the surface of the tunica intima is lined by the endothelium, which consists of simple squamos epithelium and covers the lumens of the entire vascular system [9]. The endothelium has been shown to be involved in e.g. electrical signalling in the microvascular system [11, 12], vascular remodeling as a response to shear stress [13], and has generally been shown to be influential in the regulation of blood flow [8]. Second, the tunica media consists of a circular layer of smooth muscle cells (SMC), which modulates the internal diameter of the vessel lumen and thereby regulates the blood flow through the vessel [9].

The model in this project is designed to simulate network adaptations in skeletal muscle tissue, where capillaries can be described as continuous: They have complete endothelia with tight junctions between the endothelial cells (ECs), allowing for exchange of small molecules, e.g. oxygen. Two other types of capillaries exist, of which the endothelium is not as complete in its coverage of the vessel [9].

1.2 Mean arterial pressure

Mean arterial pressure (MAP) is the mean pressure throughout a cardiac cycle, i.e. weighted between diastolic and systolic pressures in the aorta. Mean arterial pressure in humans is about 100 mmHg (about 13300 Pa) from the time of adolescence [1]. The blood pressure decreases slowly from the aorta, through the elastic arteries and the muscular arteries, and drops markedly through the through the arterioles, where resistance to blood flow due to the small lumens slow the flow of blood. The blood enters the capillaries with pressure of about 30 mmHg (4000 Pa) and leave the capillaries with about 15 mmHg (2000 Pa), then continuing through the veins with a stable low pressure [9]. As mentioned, mammals generally have a MAP of about 100 mmHg [2].

1.3 Transport of oxygen

Oxygen is carried in the blood in twos states: Bound to haemoglobin and free in plasma. Haemoglobin (Hb) is an allosteric protein to which four oxygen molecules can simultaneously bind reversibly, forming oxyhaemoglobin, making it possible to release oxygen for the tissues. Haemoglobin exists in two states: A tense state, which has a lower affinity for oxygen, and relaxed state, which has a higher affinity for oxygen. However, if oxygen binds to haemoglobin in the tense state, the protein will change conformation and more oxygen can bind more easily, which affects the relationship between the saturation of haemoglobin and partial pressure of oxygen in the blood. Since haemoglobin can only bind four oxygen molecules at the same time, the binding is limited and the proteins can become saturated. The relation between partial pressure and saturation of oxygen can be described by a saturation curve [14].

Blood usually contains a concentration of haemoglobin of 15 g/dL blood and a theoretical oxygen carrying capacity of 1.39 mL O_2/g Hb (Hüffner's constant), often empirically estimated to 1.31 mL O_2/g Hb [14]. Because of oxygen being transported both bound to haemoglobin and as free molecules, the total arterial content of oxygen in blood can be calculated as [14] :

$$C_{O_2} = (Hüffner * [Hb] * S_{O_2} * 0.01) + solubility * P_{O_2} \tag{1}$$

where S_{O_2} is the saturation of haemoglobin in %, P_{O_2} is the partial pressure of oxygen, $solubility$ is the solubility of oxygen at body temperature, Hüffner is the Hüffner constant and [Hb] is the concentration of haemoglobin. In the equation, the first term denotes the amount of oxygen carried by haemoglobin, while the second term denotes the amount of oxygen in a free state.

1.4 Tissue oxygenation and metabolism

In the microcirculation, oxygen diffuses from the blood in the capillaries to the surrounding tissues. In the creation of a tissue supply model for this project, inspiration has been found from the Krogh cylinder model [15]. Krogh [15] described capillaries as each being surrounded by a cylinder of tissue to which they deliver oxygen independently of other capillaries. Oxygen would then diffuse into the tissue as a result of oxygen pressure differences between the center of the capillary and a given location in the tissue.

The diffusion of oxygen can be described by Fick's law [14], which describes the movement of particles from a high concentration to a lower concentration [14]:

$$J = -D\frac{\delta C}{\delta x} \tag{2}$$

In the above equation, J is the diffusion flux (amount of substance per area per time), D is the diffusion constant (area per time) and x the diffusion distance (length). The diffusion over a capillary wall can be described as [14] :

$$flux = \frac{DA(C_1 - C_2)}{T} \tag{3}$$

where D is the diffusion constant for a gas a specific temperature (affected by molecular size, charge and lipid solubility, which is however not included in this model), $C_1 - C_2$ is the concentration gradient across the membrane, which can also be expressed as partial pressure, and T is the capillary wall thickness. In the capillaries, oxygen moves down the gradient between the partial pressure of oxygen in the blood and in the tissue [14]. Blood enters the capillaries with an arterial partial pressure of oxygen of about 90 mmHg [16] - 100mmHg [9] (12000 Pa - 13332 Pa), which drops to about 40 mmHg in the postcapillary vessels [16] as the oxygen is exchanged with the tissues. The partial pressure of oxygen in tissue is regulated by blood flow, availability of oxygen and consumption rate [16]. According to one review [16], skeletal muscle oxygenation generally ranges from 7.5 mmHg to 31 mmHg (1000 Pa to 2800 Pa).

Oxygen consumption is the amount of oxygen consumed by the tissues within a timeframe [14]. Normal oxygen consumption (adult male breathing at sea level at rest) is 254 mL/min [14]. Exercise can increase the oxygen consumption, and at highest possible work intensity, the bodily consumption of oxygen can (in a moderately fit subject) increase to about 3000 mL/min [17].

The amount of oxygen denoted by in partial pressure or concentration can be calculated from one to the other by Henry's law [18]:

$$\alpha_X = \frac{[X]}{P_X} \tag{4}$$

where α_X is the solubility coefficient of the gas X, [X] the gas content and P_X the partial pressure of the gas.

1.5 Mechanisms of flow regulation

Blood flow is locally controlled by a variety of mechanisms, such as autonomic nervous stimuli, different types of stress on the vessels and metabolic responses [8]. In this project, two mechanisms are included: Shear-dependent responses and conducted vascular response. In this section, main effects and aspects of the two are described.

1.5.1 Shear stress

Shear stress (SS) is a frictional force that emerges when the blood flows along the endothelial surface. This causes a deformation of the endothelial cells in the direction of the blood flow [19]. Given the

radius (r), length (l) and pressure difference (ΔP) across a vessel, wall shear stress (τ) can be calculated as [8]:

$$\tau = \frac{\Delta P r}{2l} \tag{5}$$

The above equation is derived from Pouseille's equation [8] and is therefore appropriate for Newtonian liquids (i.e. liquis that do not change viscosity with altered flow rate [19]) and laminar flows.

The exact chemical signaling pathways resulting from shear stress is not within the scope of the model in this project and will therefore not be described thoroughly. In brief, the shear stress activates surface molecules on the endothelial layer, which actives a range of chemical pathways that result in vasodilatation [13]. This means that an increase in shear stress, which can for example be cause by a larger flow through a vessel or change in viscosity [20] (of which viscosity is however not included as a variable in the present model), will cause a vasodilatation.

1.5.2 Conducted vascular response

A conducted vascular response (CVR) is a dilatation or constriction of vessels caused by an electrically transmitted signal initated by a local stimulation. The signal can travel bidirectionally along small blood vessels in the microcirculation and causes changes the membrane potentials (V_m) of the cells it goes through. The response is conducted via the cell membrane of ECs and SMCs in the vessel wall [21], where it travels through gap junctions between the cells, allowing ions to move from cell to cell with low resistance [22]. The signal can travel up to several millimetres. This means that the signal can cause vascular changes in the upstream vessels, which can be necessary for a sufficient supply of oxygen to the tissues, and allows for a coordinated response between a large number of cells [22]. Some studies have modelled the EC and SMC with a resting membrane potential ($V_{m_{rest}}$) of about -40 mV [11]. The spread of a hyperpolarization causes a vasodilatation, while the spread of a depolarization causes vasoconstriction. When a membrane potential change is conducted through the vessel membrane, the magnitude of the change will decay the further the signal travels from the stimulus site. This is caused by dissipation of current through the membrane perpendicular to the vessel length. Thereby, the membrane potential change can only be conducted a certain distance [21].

The decay of the membrane potential change is higher at branch points than through the vessels. At branch points, the mass and capacitance of one vessel will change when it divides into two smaller vessels, and the magnitude of the signal will therefore decrease [11].

Studies [23] have found that changes in oxygen tension in the tissues result in a CVR, which is transmitted to the blood supplying arterioles. This means that tissue hypoxia would cause a vasodilatation and tissue hyperoxia a vasoconstriction. This response resulting from the tissue oxygen tension is pointed out by several studies [8, 12, 23] as necessary for ensuring a correct blood flow to oxygenate the tissues.

1.6 Energy cost from maintaining blood flow (PV-cost)

One of the main questions asked in this project is: How much energy does it cost to force the blood through the modeled microvascular network?

In a pipe, the energy cost is proportional with the energy drop between two cross-sectional areas. Given the known pressure difference in the system, ΔP, it can be argued that ΔP encapsules the energy loss, which originates from resistance of friction and the divergence of the vessels in the system [24][1]. In that case, the energy loss from the flow through the pipe system can be described as [24]:

$$W_{heat} = Q\Delta P \tag{6}$$

where W_{heat} is the energy loss in watt, Q is the blood flow in the given vessel and ΔP is the pressure difference between two cross-sectional areas of the pipe. For the rest of the report, this is named the PV-cost, given the relation between the pressure and volume of blood that flows through the network.

1.7 Laminar flow and turbulence

Blood usually moves as a laminar flow, which means that the flow runs parallel to the vessel length in concentric layers and with the highest velocity in the center of the vessel and the lowest velocity adjacent to the vessel wall [19]. If the flow velocity becomes to high (defined by the viscosity), the flow can become turbulent and "chaotic". To decide whether the flow is turbulent, Reynold's number can be calculated from the characteristic length) (here the diameter d), viscosity (μ) and density (ρ) of the fluid) [25]:

$$R_e = \frac{d\rho v}{\mu} \tag{7}$$

If $R_e > 2500$, the flow becomes turbulent. Otherwise, the flow is laminar [25].

1.8 Matrix equations

Matrix equations are used in the project to calculate the blood pressure in the network and are therefore briefly introduced here. Given a linear equation system with n equations with n unknowns, the coefficients for the unknown values in each equation can be written as rows in a square matrix A, and the unknowns in a vector x:

$$\mathbf{A}\,\mathbf{x} = \mathbf{b} \tag{8}$$

where b is a vector of known values. The equation has one solution if the system cannot be reduced to fewer equations than the number of unknowns. The square matrix A is then regular and the equation can be solved [26, 27].

[1] See minor elaborations in Appendix A

2 Methods

In this section, the translation from biological system to computational model is described. To begin with, the biological system in focus will be outlined. Afterwards, the methodology of representing each element of the system is described. In the end, this will be collected into a description of the computational flow along with computational considerations. Finally, the methodology of a sensitivity analysis is presented. Assumptions about the biological system are presented in context with the part of the model they belong to.

In general, the creation of a model is a circular process: Many of the elements and parameters have been adjusted through trials and tests. Some of these tests and their conclusions are presented in these sections to describe the methodological considerations and procedures. All constants used the model are represented in Table 1 at the end of the methods section.

2.1 Overview of biological system

The main idea of the biological system, which the model should simulate, is based on the theory described in the previous section and can be described as follows (and is illustrated in Figure 1): The microvascular network is shaped as a bifurcating, symmetrical network with a number of branching vessels around the capillaries as modeled by Jacobsen et al [28]. Blood runs through the vessels from one inlet vessel with a certain inlet pressure (P_{in}), through the network, and exits the network from the other end from an outlet vessel with a lower outlet pressure (P_{out}). In the middle of the network, the blood reaches the capillary beds. Here each simulated capillary supplies a slab of tissue with oxygen. If the tissue is hypoxic or hyperoxic, a CVR is initated in the endothelium of the oxygen supplying capillary and propagated bilaterally from the initiation point, causing a change in membrane potential in the vessels and thereby a potential SMC tension change. At the same time, changes in shear stress in larger vessels can cause changes of the internal radius. The network should therefore be able to regulate the amount of blood conducted to each capillary and tissue slab by controlling the blood flow in the arterioles and precapillary arterioles further upstream and downstream in order to end up with a final network configuration that allows for a sufficient blood flow through all capillaries. Finally, the PV-cost and E-cost of the network is calculated.

Although the model is in general tissue non-specific, the model is thought to simulate skeletal muscle tissue. Skeletal muscle was chosen as specific tissue based on the large increase in metabolism due to physical exercise [17]. The work intensity (WI) variable is therefore based on physical activity, and values for acceptable partial pressure of oxygen in skeletal muscle were chosen to simulate the oxygen supply in tissues.

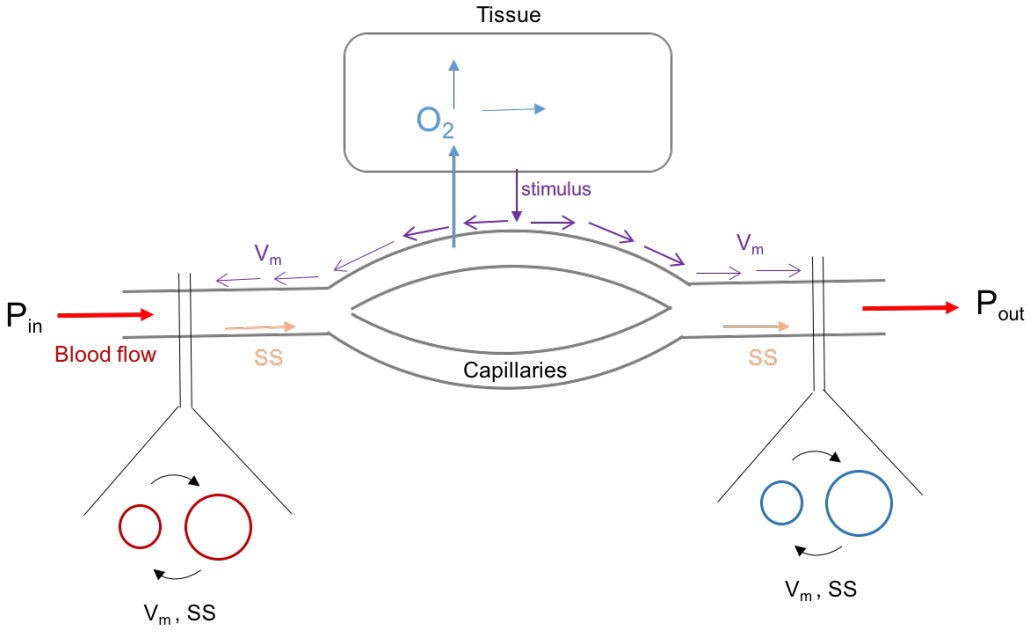

Figure 1: Illustration of the mechanisms in a small part of the modelled network. Blood (red arrows) flows from left to right at an with a pressure drop from P_{in} to P_{out}. Oxygen is delivered to the tissues (blue arrows), which can in turn initiate a CVR which travels through the endotheliam membrane (purple arrows). Shear stress (SS) affects the vessel wall (beige arrows). Membrane potentials (V_m) and shear stress affect the interval radii of the vessels.

The model of this system can be described as three sub-models put together: 1) The modeling of the vascular network with calculations of pressures and flows in the branch points and vessels, 2) a tissue supply model, which simulates the supply of oxygen from a capillary to a single slab of tissue, and 3) the regulation of oxygen supply to the tissue. Each of these three will be described in turn in the next sections.

2.2 Sub-model 1: The vascular network

The microvascular system is modelled as a symmetric network of edges (vessels)[2] and nodes (vessel branching points). Each vessel is assigned a radius and length by which the conductance of the vessel (C_j) is calculated. The inlet and outlet node are each assigned an constant pressure (P_{in} and P_{out}), respectively. The size of the network is defined by the number of generations (levels of vessel on each side of the capillaries). The example below shows a network of three generations:

[2]In the rest of the report, the edges will be mentioned as vessels as they represent the structure and properties of vessels.

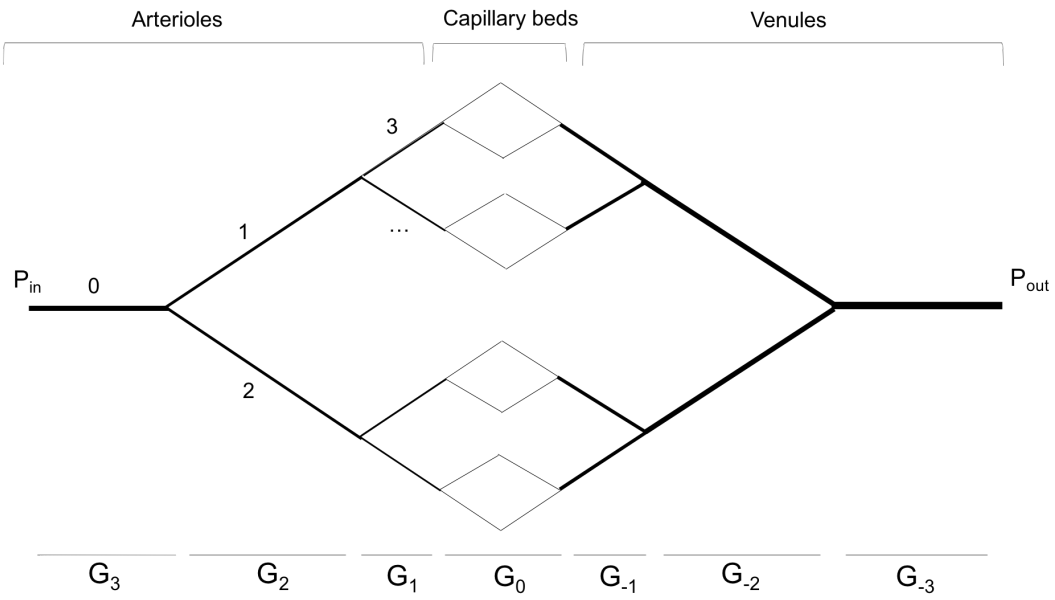

Figure 2: Example of the bifurcating network with 3 generations. Internal diameter is illustrated by thickness of edges. Inlet and outlet nodes are assigned pressures P_{in} and P_{out}. The generation (G_i) naming is showed below the network.

In the above figure, all vessels to the left of the symmetric middle axis represent arterioles, and vessels to the right represent venules. The middle vessels (generation 0) represent capillaries. Two capillaries that branch from the same artery and enclose into the same vein are from hereon mentioned as (capillary) *beds*. The arterioles and venules are named by their generations, e.g. generation 2 (G_2) and -2 (G_{-2}) respectively. When simulating the network, a variable inlet pressure, P_{in}, enters the network from the arteriolar side. The rightmost node is simulated with an outlet pressure, P_{out}, of 15 mmHg (2000 Pa) based on the outlet pressure of similar models (e.g. [7]). All vessels are assigned an index (the numbers by the vessels, Figure 2) which are used throughout the computational simulations.

A flow, Q, in a pipe can by Ohm's law be calculated as the product of the conductance and pressure difference at the ends of the pipe:

$$Q = C * \Delta P \tag{9}$$

Based on Kirchoff's law, which says that the sum of flows to and from a node is equal to zero, the flow through a node can be calculated as [28]:

$$\sum_j Q_j^n = \sum_j C_j^n \Delta P_j^n = 0 \tag{10}$$

where Q, C and P represent flow, conductance and pressure drop in vessel j entering node n. Additionally, it is assumed that the flow is laminar and that blood is Newtonian, i.e. viscosity doesn't change with velocity [19], Pouseille's law can be applied for conductance [28]:

$$C_j = \frac{\pi r_j^4}{8\mu l_j} \tag{11}$$

where r_j and l_j is the radius and length of the vessel j and μ is the viscosity of the blood. Given the network as shown in Figure 2, this means that the flow through e.g. P1 (first node after inlet node) can be described as:

$$Q_1 = C_{in} * (P_{in} - P_1) - C_1 * (P_1 - P_2) - C_2 * (P_1 - P_3) = 0 \tag{12}$$

which can be rearranged to

$$-P_{in} * C_{in} = -P_1 * (C_{in} + C_1 + C_2) + P_2 * C_1 + P_3 * C_2 \tag{13}$$

When similar rearrangements are performed for the flows in through all nodes, the following matrix equation can be obtained (in this example, only a small network with 1 generation apart from capillaries is included):

$$\begin{bmatrix} -(C_{in} + C_1 + C_2) & C_1 & C_2 & 0 \\ C_1 & -(C_1 + C_3) & 0 & C_3 \\ C_2 & 0 & -(C_2 + C_4) & C_4 \\ 0 & C_3 & C_4 & -(C_{out} + C_3 + C_4) \end{bmatrix} \cdot \begin{bmatrix} P_1 \\ P_2 \\ P_3 \\ P_4 \end{bmatrix} = \begin{bmatrix} -C_{in} P_{in} \\ 0 \\ 0 \\ -C_{out} P_{out} \end{bmatrix}$$

which can be solved with linear algebra to find the pressure values in each node apart from P_{in} and P_{out} ($P1$, P_2, etc.). This is done in Python with the Numpy package.

2.2.1 Vessel features

Before the simulations, each vessel in the network is assigned a length and an internal radius. The vessel length is dependent on the generation to which the vessel belongs and computed as [28]:

$$l = k_1 * e^{k_2 * |g|} \tag{14}$$

where g is the generation of the vessel and k_1 and k_2 are constants (see Table 1). Capillaries are assigned a total length of 100 μm (50 μm arterial and venous side, respectively). The remaining vessel lengths vary exponentially: The vessels far from the capillary bed are longer than vessels close to the capillaries. This pattern is uniform on the arterial and venous side.

The vessel radii were computed from the following equation based on Murrays law [28]:

$$r = k_3 * (2^{|g|-1})^{\frac{1}{k_4}} \tag{15}$$

where g again denotes the generation of the vessel, k_4 is a constant and k_3 denotes the offset value which is specific for arteries (pre-capillary arterioles: r = 6 μm) and venes (post-capillary venoules: r = 15 μm). Note that by radius this means the internal lumen radius. The vascular wall is not included in this model.

Throughout the simulations, all radii except in capillaries can decrease or increase due to signalling feedback in the network, but lengths are constant throughout the simulation. Since capillaries do not have a layer of SMC [9], their radii do not change.

To avoid simulating a deterministic system, a stochastic element is introduced in the model. This is done by adding noise ϵ to the lengths and radii otherwise assigned by the equations 14 and 15. The noise is drawn from a normal distribution (μ = 0, sd = 0.1), where the standard deviation is based on findings for capillary size variation [29]. The noise thereby adds or subtracts a fraction of the original vessel radius r_j or length l_j from the given feature:

$$l_j = (1 + \epsilon) * (k_1 * e^{k_2 * |g|}) \tag{16}$$

$$r_j = (1 + \epsilon) * (k_3 * (2^{|g|-1})^{\frac{1}{k_4}}) \tag{17}$$

The noise is assigned to all vessels, including the capillaries. However, since each capillary is represented by two edges in the network, these two edges are assigned the same noise to the radii and lengths, respectively, so that one capillary keeps the same radius throughout its length and the middle of the capillary is placed at the node between the two edges. Although the magnitude of the noise caused some deviation from comparison to Murray's law, no other clear references were found on the variation of blood vessel size and the variation size was kept.

2.3 Sub-model 2: Tissue oxygenation

In short, the tissue oxygenation submodel is a representation and simulation of a virtual capillary supplying a tissue slab with oxygen. The section also covers the geometrical considerations, equations and estimation of parameters.

2.3.1 Visual representation and geometry

The model simulates a virtual capillary of constant length 100 μm and radius 5 μm supplying a virtual cylindrical tissue volume reaching 30 μm out perpendicular to the capillary (see Figure 3). Note that the length and radius for the capillary is constant, while changes in flow are represented by virtual radii, which is described later. It is assumed that each cylindrical tissue volume is supplied by only one capillary.

Although the model represents this three-dimensional physical entity, the virtual model is made up by a two-dimensional grid representing the capillary and a slab of the tissue around the capillary (see Figure 3). This virtual slab represents 1/8 of the total volume of tissue supplied with oxygen by the capillary, and is divided into three horizontal layers parallel to the capillary of each 10 μm height, which are each divided into ten grid cells.[3] It is assumed that the tissue acts as a homogenous medium (no simulations of cell walls, cytoplasm, variations in metabolism or other specific entities). This means that the placement of cells and membranes are not taken into account and simplifies the

[3]NB: The term "cell" will throughout the report be used to describe the grid spaces in this model. "Cell" does therefore NOT indicate an actual biological cell.

modeled diffusion patterns. The increasing volume of the three-dimensional tissue space is simulated by using virtual volumes and areas between cells when computing the amount of oxygen in the cells. The calculations as described in the next sections therefore take the cell layer's volume and surface area into account.

Henceforth, the simulated grid of capillary and tissue will be referred to as a *supply unit*. The next section will describe the modeling of oxygen content in the capillary blood, and afterwards the movement of oxygen from the capillary to and in the tissues is clarified.

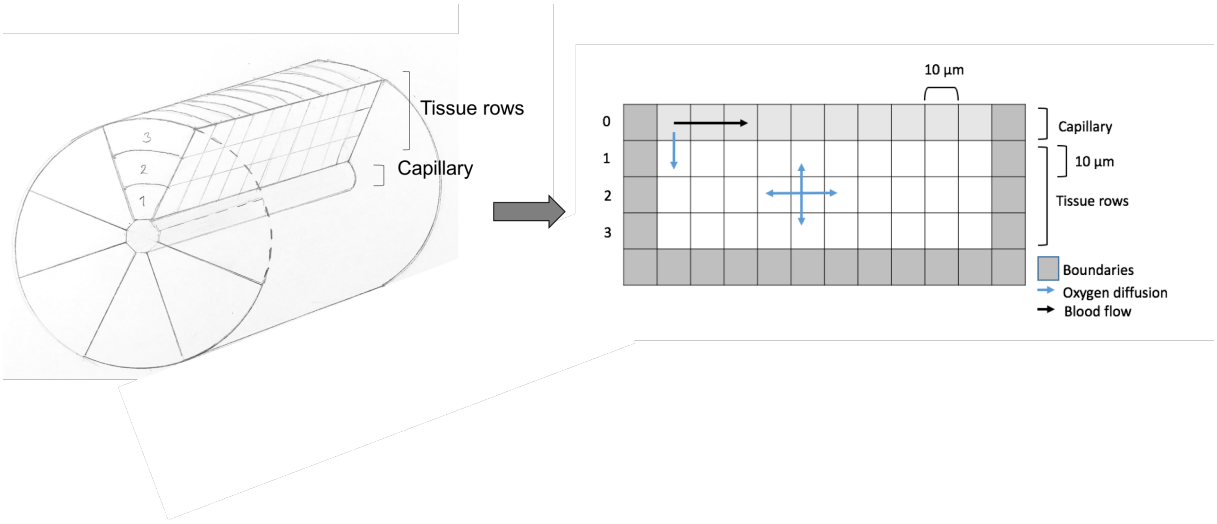

Figure 3: Illustration of the conversion from a 3D cylinder of tissues supplied by a capillary to the 2D matrix system that represents the capillary. Note that the matrix represents an eighth of the actual cylinder. Blood flow direction and oxygen diffusion directions in the are shown with black and blue arrows.

2.3.2 Flow velocity and time steps in the supply unit

The movement of blood and oxygen in the model is modelled as discrete changes in each matrix cell for each iteration. The model is thereby designed as a discrete model with time steps of 10 ms. This discrete structure was chosen to easily set a limit to the number of cells in the supply unit, since more cells come with a higher computational cost during simulations. However, it is assumed that with such small time steps, the spread of oxygen in the tissue approaches the otherwise continuous development in vivo.

Previous experiments [30] have measured capillary blood velocity to 0.79 mm/s for capillaries with a diameter of 2-5 μm. In this model, this is simplified to 1 mm/s = $1.0 * 10^{-3}$ m/s. Given the length of the capillary (100 μm), the blood travels through a capillary in 100 ms and moves from one capillary cell to another in 10 ms. It should be mentioned that although time is not a factor of interest with regards to progression towards equilibrium in the overall model, it is used in this sub-model to convert the flows calculated by the network matrix to blood volumes (will be described later) and to estimate the amount of diffusing oxygen.

2.3.3 Oxygen content in capillary blood

The capillary blood is simulated as entering the capillary with a partial pressure of oxygen of 100 mmHg (13332 Pa). To calculate the saturation of the blood, an equation for the oxygen dissociation curve was fitted from data points produced by Severinghaus [31]. The data points include values for P_{O_2} (in mmHg, therefore first converted to Pa) and percentage of saturation and reflect oxygen saturation in human blood at $37°C$ and pH = 7.4. The fit was executed in R with the nonlinear least squares function (nls()). This resulted in the following logistic function for oxygen saturation (SO_2):

$$S_{O_2} = \frac{96.8390}{1 + e^{-\frac{1}{1265.3844}(P_{O_2} - 3684.1381)}} \tag{18}$$

making the asymptote saturation 96.9%, a logistic growth rate of $1/(1277.0102$ Pa), and about 50% saturation at partial pressure level P_{O_2} = 3683.5459 Pa (27.6 mmHg). The resulting curve deviated slightly from the data observations, especially not reaching as low a saturation at low partial pressures as denoted in the data. However, since partial pressures below 2666 Pa (20 mmHg) are not expected in the virtual capillary, the result was deemed acceptable for the model.

Equation 18 is used to convert the partial pressure of oxygen in the capillary blood to the corresponding saturation level. The concentration of oxygen can then be computed by:

$$C_{O_2} = (Hüffner * [Hb] * \frac{S_{O_2}}{100}) + (solubility * P_{O_2}) \tag{19}$$

Parameters for the equation is found in Table 1. However, in the reverse calculation (conversion of concentration to partial pressure) the inclusion of the free oxygen molecules (represented by the second term in equation 19) causes impossible mathematical values, this term is excluded from the model. Since the amount of free oxygen is only a minor fraction of the total oxygen content, it is estimated that this exclusion of free oxygen from the calculations will not have an overall effect on the final model. The reverse function is then found by calculating saturation from the first term in equation 19 and then solving for partial pressure in equation 18.

2.3.4 Oxygen movement

In the supply unit, the movement of oxygen is simulated in two ways: First of all, a large part of the oxygen in the blood follows the blood flow through the capillary cells by convection. Second of all, oxygen diffuses from the capillary to the tissue and between tissue cells.

The supply unit grid (see Figure 3 to the right) is computationally modeled as a matrix indexed with the capillary being *row 0*, and the remaining rows as tissue layers *1, 2* and *3*. Each row is divided into ten cells (index *0-9*).

As mentioned, oxygen enters the supply unit through the arteriolar end of the capillary (capillary cell [0]) with a fixed partial pressure of Pa_{O_2} = 100 mmHg (13332.24 Pa). It is assumed that no oxygen leaves the blood from other vessels than the capillaries. In the subsequent iteration, oxygen diffuses from this capillary cell to the adjacent cell in the first tissue layer. The amount of diffused oxygen is calculated with Ficks law (equation 2) based on the difference in partial pressure between the cells. The full equation for flux, based on equation 3, is:

$$flux = \frac{\gamma_1 DA\alpha\Delta P}{L} * t \tag{20}$$

where flux is the moving volume of oxygen, γ is a unitless modification parameter (see Table 1), D is the diffusion coefficient, A the area of diffusion, α the solubility constant, ΔP the pressure difference between two matrix cells, L the diffusion length and t the time step of the model (10 ms).

Because equation 20 refers to the flux of oxygen from the capillary and to one slab of tissue out of eight in the tissue cylinder, the flux volume is then multiplied by eight and subtracted from the volume of oxygen corresponding to the partial pressure of oxygen in the capillary cell. The flux (corresponding to flux to one tissue slab) is added to the adjacent tissue cell. The resulting oxygen volume in the capillary cell is converted back to partial pressure and "transported by convection" to be the new Pa_{O_2}-value for the next capillary cell (capillary[1]). Thereby, the partial pressure pressure in a capillary cell i at iteration t can be described as:

$$Pa_{O_{2i}} = 100mmHg, \qquad i = 0 \tag{21}$$

$$Pa_{O_{2i,t}} = Pa_{O_2}(V_{i-1,t-1}), \qquad i = 1..9 \tag{22}$$

where V is the volume of oxygen in a capillary cell and $Pa_{O_2}(V)$ is the partial pressure of oxygen corresponding to that volume.

In the tissue rows, oxygen in one cell can move to and from all four surrounding cells depending on the flux defined by Fick's law (equation 20). Because the state of the tissue slab (the tissue rows of the 2D-matrix, see Figure 3) represents the development in one of all eight slabs around the capillaries, the oxygen is assumed to only move perpendicularly and in parallel to the capillaries (allowing for the 2D-matrix system). Before the flux of oxygen is calculated, the amount of oxygen consumed by the tissues is subtracted. For each timestep, the change in oxygen level in one cell from fluxes and metabolism can be described as:

$$\Delta O_2 = \sum_{i=1}^{4}(F_{O_{2_i}}) - M_{O_2} \tag{23}$$

where $F_{O_2 i}$ is the flux from each adjacent tissue cell i, and M is the metabolism in the cell (described in the next section).

As the oxygen diffuses towards the borders of the slab (see Figure 3, the diffusion area between cells and cell volume increase while the remaining parameters stay unchanged. This was done to simulate the diffusion of oxygen in an in vivo three dimensional structure. To simulate that the supply unit is surrounded by other "independent" supply units, the tissue matrix is modeled with an outer grid frame with the same pressure values as the adjacent tissue cells (see Figure 3), since it was assumed that the same diffusion process occurs in the "adjacent" tissue slab, and that no diffusion in or out of the modeled slab would happen.

The conversion between concentration and partial pressure of oxygen in the tissue cells is done according to Henry's law (equation 4). The solubility constant (see Table 1) was taken from studies which have approximated the solubility of oxygen in skeletal muscle tissue [29].

2.3.5 Oxygen consumption

Oxygen consumption in the tissues is modelled based on work intensity (WI) and typical estimated values for oxygen consumption.

Metabolism based on WI is modeled as a linear function of work intensity in per cent. The function is created based on a metabolism in skeletal muscle of 75 mL/min at rest (WI = 0%) and a bodily consumption of 3000 mL/min at highest possible intensity (WI = 100%) [17], with the assumption that most of this high consumption is due to skeletal muscle activity.

The linear function was calculated based on the assumption that about 30 L of 70 L body could be skeletal muscle tissue, roughly estimated from the skeletal muscle constituting about 40% of body mass [1]. An intercept and slope for the linear function was thereby calculated and resulted in the following equation:

$$M_{max} = \frac{7}{432000}\frac{m^3}{s} * WI + \gamma_2 * \frac{1}{21600}\frac{m^3}{s} \tag{24}$$

where $M_{max}(WI)$ is the metabolism in m^3O_2/s. γ_2 is added as a parameter to adjust for effects from non-included physiological processes and properties - e.g. exact tissue volumes, tissue content, etc.

This maximum metabolism rate is used to calculate the actual metabolism in the grid cells, which follow Michaelis-Menten kinetics. The Michaelis-Menten kinetics was chosen in order to ensure that if there is no oxygen in the cells, there will be no consumption. Studies [29] report the use a critical P_{cr} = 0.5 mmHg which is also used in this model. In general, it is the case that $P_{O_2} >> P_{cr}$. The consumption of oxygen in a cell therefore depends on both WI and the P_{O_2} in the cell.

The actual consumption in each grid cells is therefore defined as:

$$M(P_{O_2}, WI) = \frac{M_{max}(WI) * P_{O_2}}{P_{O_2} + P_{cr}} \tag{25}$$

where $P_{O_{2t}}$ is the partial pressure of oxygen in the particular cell and P_{cr} is the critical P_{O_2} denoting a consumption rate of 50% of M_0. In the simulations, consumption of oxygen is simulated before the diffusion - in other words, it is assumed that the tissue uses the oxygen it needs before the oxygen diffuses away. If the amount surpasses the amount of oxygen present in a cell, the oxygen level in the cell is set to 0 with an if-statement to avoid negative values of oxygen to interrupt the diffusion patterns.

All tissue cells in all supply units are assigned the same maximum metabolism rate, since it is assumed that the network supplies a volume of tissue with the same task and work intensity. This assumption was made due to the small size of the microcirculation [10]. However, the metabolism per cell for each iteration is computed from the partial pressure of oxygen in the respective cells.

2.3.6 Simulation of capillary flow changes

As mentioned, simulation of oxygenation of a tissue slab happens with a constant capillary radius, length and blood flow velocity. At the same time, changes in network configurations (due to changed in V_m and shear stress) can lead to a higher flow in the capillaries in order to supply more oxygen.

Increased flow in the capillaries is simulated in the tissue supply sub-model as an increased virtual volume in the capillary cells. When a capillary flow, Q_{cap}, has been computed based on the conductance in the vessel and pressure differences in the nodes around the vessel, the size of the virtual volume of blood, $V_{virtual}$ can be calculated based on the virtual cross-sectional area, $A_{virtual}$ of the capillary, which can be calculated from the simulated flow (Q_{cap}) and the "constant" velocity of capillary flow (v_{cap} of 1 mm/s:

$$V_{virtual} = A_{virtual} * L_{cap} = (\frac{Q_{cap}}{v_{cap}}) * L_{cap} \tag{26}$$

Thereby, the virtual volume of blood in each cell can be calculated based on the length of the capillary cell. This means that a red blood cell which would normally pass faster through the capillary, will now pass at the same velocity, but a larger volume of blood is available - while the same diffusional area is kept, leading to a smaller diffusional area pr. volume. The aim is hereby to represent an increased flow while keeping the model's time step structure.

2.3.7 Validation criteria and modification of constants

When examining the model of the tissue supply unit, the following considerations of validation were made in order to let the submodel be included in the full model:

First of all, given a typical velocity of blood through the capillaries ($1.0 * 10^{-3}$ m/s) and that the geometrical parameters were comparable to an actual capillary size, it was assumed that the flow through such a capillary would be sufficient or more than sufficient for a resting muscle, while a hard working muscle would require a larger flow. It was therefore expected that at WI = 100%, the tissue slab would eventually lack oxygen, while at WI = 0%, the tissue would possible be overflown with oxygen. When simulating the slab without any adjustments, it was evident even at WI = 100%, the tissue would be more than sufficiently supplied. Therefore the intercept of the WI function was multiplied by factors between 10 and 100. Together with examinations of the metabolism in the full model, the parameter γ_2 was selected to be $\gamma_2 = 6.0 * 10^1$.

Second of all, it was examined that the partial pressure of oxygen in the capillary blood (matrix row 0) decreased from the inlet cell (P_{O_2} = 13332 Pa (100 mmHg)) to the outlet cell. It was also checked that the cells in the tissue matrix followed a pattern with the highest oxygenated cell adjacent to the inlet capillary cell, and the least oxygenated cell in the corner furthest from this, which was found in literature to be a typical case [32]. The modification parameter, γ_1 was included to account for the effects possible biological processes that are not included in the model. It was found that if the flux was not large enough (low γ_1), the tissue cells furthest from the capillary would barely receive any oxygen. It was also found that if the flux of oxygen was too high (γ_1 too high), an increasing "flood" of oxygen would pass from cell to cell, leaving every second cell with an overload of oxygen and the remaining cells with no or negative. This was caused by a flux of oxygen from cells that surpassed the actual content of oxygen in the cell. To avoid this issue, it was found necessary that γ_1 was smaller than or equal to 1.3. This value would allow diffusion from a cell to four adjacent cells with no oxygen without leaving a negative PO_2 value in the original cell. If the value was higher, negative values of

oxygen could occur, which would cause the ”floods” of diffusion.

Third, it was examined that given no metabolism, the tissue would eventually be filled with oxygen. This was found to be the case for the above conditions.

2.3.8 Overall tissue supply algorithm

To sum up the process of the above calculations, a brief description of the tissue supply algorithm is shown in Figure 4. When a supply unit is updated for each time step, oxygen moves between matrix cells (see Figure 3). Oxygenation states in one timestep is moved from an ”old matrix” with PO_2 values for each cell to a ”new matrix” with PO_2 values for the next time step. While diffusion is based on differences in partial pressure between cells, the actual flux is calculated as the corresponding volumes of oxygen which are subtracted and added to the appropriate volumes of oxygen in the cells.

During the simulation step, each update of the tissues will end with an evaluation of the oxygen level in the tissues. The evaluation is based on cell in the tissue grid with the *lowest* P_{O_2}. This is described further in the next sections, which cover the mechanisms that cause remodeling in the network.

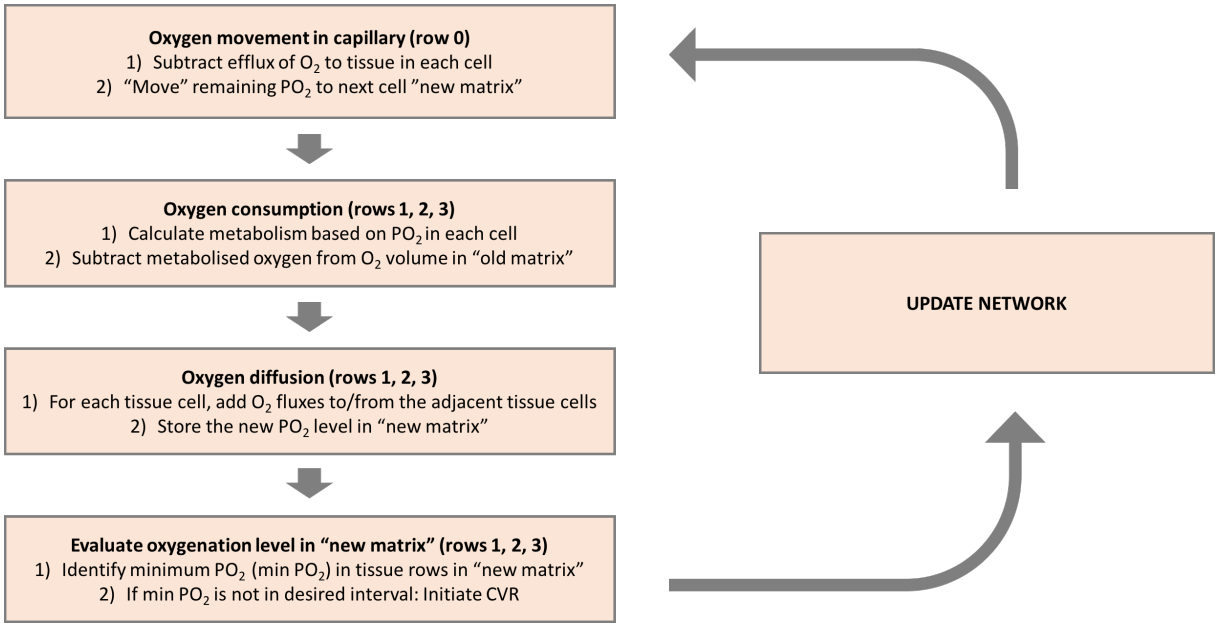

Figure 4: Flow of tissue supply proces. ”Old matrix” contains PO_2 levels for each time step t-1, while ”new matrix” contains the new PO_2 levels for time step t. The process is simulated in all supply units.

2.4 Submodel 3: Flow regulation

In the model, a change in flow through vessels during a simulation is caused by a change in vessel radii. The vessel radii are as mentioned regulated by two mechanisms: Membrane potentials (CVR) and shear stress (see Figure 1).

CVR is included in the model because of the main question about the connection between metabolism and magnitude of blood pressure. As already described in the theoretical sections, CVR is in literature viewed as an important link between the metabolism needs in the tissues and the adaptation of the microvascular system [8]. However, since the electrical response can only travel a certain distance [11], the simulations hold a risk that the vessels close to the capillary beds will be highly affected (e.g. large dilation) while the vessels further upstream or downstream will not dilate due to a loss of signal. The pattern where vessels closer to the capillary have smaller diameters will can then be expected to be broken. In order to avoid such a discrepancy between the internal diameters of the inner and outer vessels, shear stress was added as a second mechanism. Given the large pressure drops in the upstream arterioles compared to the precapillaries and venules [9], the shear stress should therefore have a larger effect on the upstream arterioles than the vessels close to the capillary beds.

In the next sections, the submodels of the CVR and shear stress mechanisms are described. Subsequently, the integration of the two and the effect on remodeling is presented.

2.4.1 CVR

Although the currents provoking a CVR are conducted through both the EC and SMC layer of the vessel wall [11], the conduction model is simplified to take place in one virtual layer (a virtual EC), which directly affects the tension of the SMC. It is therefore assumed that no current is lost in the conductance from EC to SMC, and the actual SMC membrane potential is not modelled.

The simulated CVR is initiated when a tissue slab is under hypoxic or hyperoxic conditions. As mentioned, studies have found that skeletal muscle oxygenation ranges between partial pressures of 7.5 mmHg and 31 mmHg (1000 Pa and 4132 Pa) [16]. However, this allows for a large range of acceptable values, a large amount of possible vessel radius end states and a risk of a high computative runtime to possibly reach the boundaries of the interval. Therefore, the allowed range was decreased to 16 mmHg $< P_{O_2} <$ 22 mmHg with the aim of still keeping an interval of acceptable values. This interval in the middle of 7.5 and 31 mmHg was chosen in order not to favor a low or high oxygenation.

If a supply unit at a given iteration has a minimum oxygenation value outside of the ideal range, a stimulus would be "injected" in the capillary membrane (one stimulus pr. capillary) between $-1.0 * 10^{-11}$ A and $1.0 * 10^{-11}$ A, depending on the need for less or more oxygen, respectively. The stimulus was chosen as dependent on the minimum oxygen PO_2 with the assumption that the primary need for the tissue is to avoid hypoxic conditions in all tissue cells, which could have happened if a mean or corner value had been the chosen criteria. The stimulus works as an error signal and was designed to gradually follow the deviation from the ideal range in a linear manner. If the the minimum oxygen value is $<$ 7.5 mmHg or $>$ 31 mmHg, the full stimulus is "injected".

CVRs are modelled to spread in both directions. When the stimulus is "injected", the electrical potential is conducted to nodes around the vessels and then further to the next vessels. As a simplification, all vessels were simulated as having one EC membrane, which means that resistance from gap junctions is not included. This is an extremely simplified adaptation of a vessel containing an inner lining of many endothelial cells [11], but the extra complexity of calculating the amount of ECs in each vessel and thereby their individual resistance is avoided. Instead, elements such as dissipation

is calculated based on the area of the entire vessel membrane surface area.

The ECEC membranes in the model have a resting membrane potential of $V_{mrest} = -41.09420040mV$. In general, a change in the membrane potential in any one vessel (apart from capillaries, which also depend on stimuli from the tissues) depends on two factors: The current to or from the nodes at the capillary ends and the dissipation from the membrane. The change in membrane potential in a given vessel j (except capillaries) is thereby described by [11]:

$$\Delta V_j = -\frac{1}{C_m}(I_{membrane} + I_{nodes})\Delta t \tag{27}$$

where C_m is the membrane capacitance, $I_{membrane}$ is the dissipation of current from the membrane, Δt is the time (10 ms), and I_{nodes} is the sum of currents to or from the nodes around the vessel [11]:

$$I_{nodes} = C_j \sum_{i=1}^{2}(V_m - V_{N_i}) \tag{28}$$

In the above equation, C_j is the coupling conductance for vessel j between two endothelial cells whose membranes meet at in a node V_{N_i} [11]:

$$C_n = ECEC_{couplingConductance} * circ_j * L \tag{29}$$

where $ECEC_{couplingConductance}$ is the coupling conductance between two ECs, $circ_n$ is the circumference of the vessel and L is the endothelial thickness (see Table 1).

For the capillary vessels, which can be stimulated by metabolism responses, the equation for ΔV includes the stimulus term $I_{metabolism}$ [11]:

$$\Delta V = -\frac{1}{C_m}(I_{membrane} + I_{nodes} + I_{metabolism})\Delta t \tag{30}$$

The dissipation from the membrane, $I_{membrane}$, which will drag the membrane potential towards the resting potential, is computed as the current density as fitted by Hald et al. [11]:

$$I_{m_j}(V_{m_j}) = 19.59 + 0.99V_{m_j} + 1.66 * 10^{-2}V_{m_j}^2 + 1.00 * 10^{-4} * V_{m_j}^3 \tag{31}$$

where I_{m_j} is the current density from the vessel j with membrane potential V_{m_j}.

Each node is modeled as a virtual membrane with a membrane potential. This potential is calculated as the weighted average of the membrane potentials of the two or three vessels branching from the node point based on the circumference of each vessel:

$$V_n = \frac{\sum_{j=1} c_j V_{m_j}}{\sum_{j=1} c_j} \tag{32}$$

where V_n is the node potential of node n and c_j and V_{m_j} the circumference and membrane potential, respectively, of the vessel. For the outermost nodes, the node potential is set to be equal to the membrane potential of the associated vessel, so the only changes in potentials can come from within the network.

2.4.2 Shear stress

The shear stress in each vessel is calculated as:

$$SS_j = \frac{r_j \Delta P_j}{2 l_j} \tag{33}$$

as described in equation 5. SS_i, r_i, ΔP_i and l_i denote the shear stress, radius, pressure drop and vessel length of vessel i. Also the shear stress theoretically initiates chemical processes in the endothelium lining, shear stress is modeled as having a direct effect on vessel radius, which is described in the next section.

2.4.3 Radius modification

The membrane potentials and shear stress affect the tension of the SMC. Each of the two contributions to the tension are calculated as:

$$tensionPotential_{V_{m_j}} = \frac{2}{1 + e^{(-200 * (V_{m_j} - V_{mrest}))}} - 1 \tag{34}$$

$$tensionPotential_{SS_j} = -(\frac{SS_j}{SS_{0_j}} - 1) * SS_j * \gamma_3 \tag{35}$$

where V_{m_j} is the membrane potential of vessel i, SS_j the shear stress in vessel i and SS_{0_j} the initial shear stress in vessel i. γ_3 is a modification parameter to adjust SS_j to a scale of about 1.

The SMC tension effect of the membrane potential is shaped as logistic curve forming a gradual tension response between -1 and 1. This was done to ensure gradual effect. Note that a hyperpolarization leads to lower tension (vasodilatation) and a depolarization leads to higher tension (vasoconstriction). A full positive or negative influence happens at a membrane potential of about -20 mV and -60 mV, respectively.

The tension potential effect of shear stress is not centered between -1 and 1, but can possibly exceed 1 and -1. The assumed logic of this shear stress lies in its two factors: The first factor (in the parenthesis) fixes the development of the shear stress around a fixed initial value to ensure stability, and the direction of the tension effect is determined hereby. For example, if the new shear stress is higher than the initial, this will result in a lower SMC tension. The second factor, $SS_j * \gamma_3$, is added to differentiate the response between vessels with high shear stress and low shear stress. The equation is further discussed in the discussion section.

Overall, the two tension potentials lead to a change in the internal radius of the vessel:

$$r_{j_t} = r_{j_{t-1}} - r_{j_{t-1}} * variationRange * (tensionPotential_{V_{m_j}} + tensionPotential_{SS_j}) \tag{36}$$

where r_{i_t} is the new radius for vessel j and $r_{i_{t-1}}$ the radius to be updated. The *variationRange* is a percentage around which the radius changes centers. The value was set to avoid sudden extreme changes in the vessel radii. A radius can increase or decrease around a setpoint of 0.5% percent of its previous value in each time step. Note that radii are therefore updated relative to their size in the previous iteration instead of compared to their original radii. This is done in order to ensure the

development of a long-term change, while a change relative to the original value would simulate a short term change. Since there is no SMC around capillaries [9], capillary radii never change.

In the model, the effect of shear stress on SMC tension is annulled for the generations 1 and -1. This was done after several simulation trials where the effect of shear stress and membrane potential work in opposite directions and cancel each other out. In order to make it possible for the membrane potentials to be particularly efficient in the aim of correct tissue oxygenation, it was therefore allowed as the only influence on the pre-capillary and post-capillary vessels.

2.4.4 Validation criteria and modification of constants

In the studies by Hald [11], CVRs were investigated with injections of stimuli of $9.0 * 10^{-10}$ A, and initially the model was therefore testet with stimulus magnitudes of 1 nA. However, this led to extreme growing membrane potentials causing the model to collapse. The parameter was then estimated by model trials, and a stimulus magnitude of $1.0 * 10^{-11}$ A was found to be large enough to initiate a spreading current while not causing the membrane potentials to grow violently.

A similar challenge was found for the specific coupling conductance between two ECs, G_{ECEC}, which modifies the conductance of current from the vessel EC to the virtual node membrane. If this value was too high, an analysis of the three contributions to membrane potential (stimuli, current from nodes and dissipation) found that a combination of accumulation of current in the capillary membrane and too large contribution from the nodes caused the (primarily) capillary membrane potentials to grow to extreme values (potentially far above 1000 mV). Trials of ranges of values led to the diminishment of the value specified by Hald [11] (see Table 1) by $2 * 10^{-5}$. A validation criteria was applied that dissipation should be able to eliminate a polarization of the membrane potential, which was fulfilled for the final parameters.

Finally, the current density as modeled by Hald [11] was diminished by a factor 10, because the stimulus signal would otherwise quickly be eliminated, causing no change in the upstream vessels.

2.5 Computational flow and considerations

All of the above translations from biology to model elements are united into one computational program flow. The program can be divided into a *preparation step* and a *simulation step*.

In the *preparation step*, the network matrix is generated based on an inlet pressure value along with arrays with initial values for the network: r (internal vessel radii), l (vessel lengths), P (node pressures), SS (shear stress for each vessel), Vm (vessel membrane potentials), Vn (node membrane potentials), Q (flow through each vessel), $stimuli$ (stimuli) and c (vessel circumferences). The matrix is generated based on an input of number of network generations that should be included in the model. Apart from this, a WI is defined, setting a common maximum metabolism for all tissue slabs. A supply unit is generated for each capillary and "filled" with oxygen until the minimum PO_2 in the unit is above 2533 Pa (19 mmHg). This value was chosen in order to be close to the desired interval to reduce computational runtime. Metabolism is not activated in the *preparation step*. All variables and parameters are calculated in SI units.

The adaptation of the network to the metabolism rate happens in the *simulation step* in a main computational loop, where the above mentioned variables are updated for each iteration, while metabolism rate, inlet pressure and outlet pressure are kept constant. Tissue metabolism is activated, and the vessels adapt based on CVR and shear stress. The process is shown in Figure 5.

Each simulation was run until equilibrium or for a maximum of 11000 iterations. A maximum number of iterations was chosen because several trials showed that e.g. configurations with an inlet pressure that was too low would never reach equilibrium. Additionally, the simulation of the network was found to be computationally heavy and of long duration.

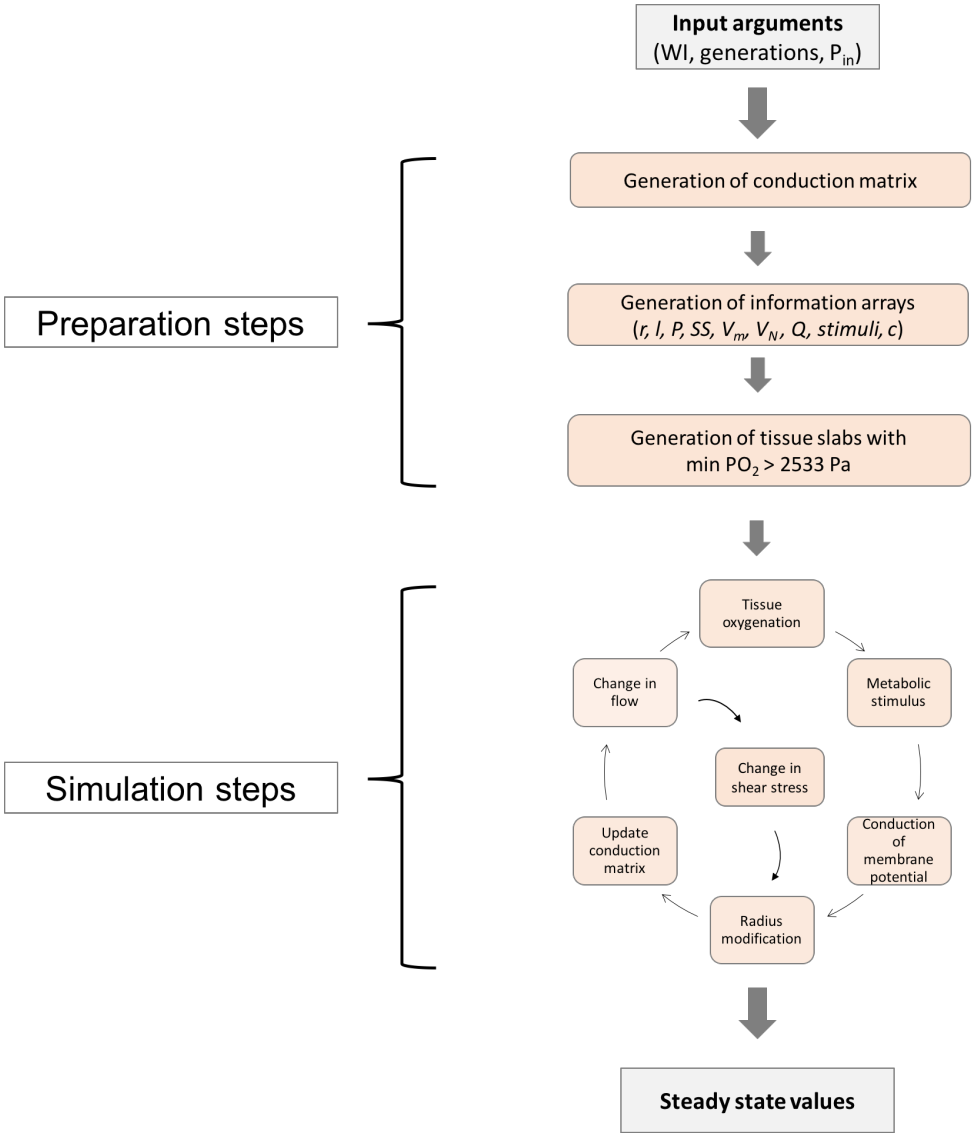

Figure 5: Computational flow for a simulation of a network for a given P_{in}. Note that although shear stress is part of the circular iteration process, but placed between ”Change in flow” and ”Radius modification” to illustrate its effects.

Equilibrium was defined as the time step where the network states (e.g. radii) matched the network state 2000 iterations earlier and when the membrane potential matched the resting potential:

$$\delta = |\frac{stateArray_{i-2000}}{stateArray_i} - 1| < 10^{-3} \tag{37}$$

$$-42.5mV < V_m < -41.0mV \tag{38}$$

The above equilibrium condition was demanded for the vectors V_m, radii and V_n. Shear stress (SS) and flow (Q) were also desired for use, but due to computational issues the vectors were disregarded. However, if equilibrium was not reached, the simulation progressions were still inspected visually, since cases of minor oscillations or membrane potentials in en equilibrium different than the resting potentials were found to occur.

The scripts for the simulations were written in Python (version 3.6.6). Since the program contains a high number of iterations (through supply unit cells, tissue slabs and timesteps), the NumPy package was utilized for array operations and linear algebra. A few operations were done in R (version 1.0.153) for fitting of functions to data.

2.5.1 Generation of results

In each simulation, the network was run with the same configurations for radii and length with a number of different inlet pressures in order to find the effect of inlet pressures. The results for three different configurations were found in order to compare the results and identify possible variations in the output. Most results were based on a work intensity of 50%, as it was assumed that the network would have to perform adaptations in case of both low and high inlet pressures.

2.5.2 Time

Time steps play a functional role, but not an evaluating role in the model. In the tissue supply sub-model, time is included as a mean of calculating the amount of diffusing oxygen across capillary and tissue grid borders. Also, it is used to calculate the amount of blood in each capillary field as a representation of variable blood flow velocity. In order to follow this "flow" of simulated oxygen, the rest of the model follows the very same time steps, which is set to 10 ms. However, time should not be used for interpretation of results: For example, although equilibrium is reached after 6000 iterations – corresponding to 60 seconds – this does not mean that the model suggests a vascular remodelling process that is over in 60 seconds. Since the final state of the network is of primary interest in this project, and since the computational load is heavier the more virtual tissue slabs are included, a realistic time scale has not been chosen to be within the scope of this model.

2.6 Energy costs: PV-cost and E-cost

Based on equation 43, the PV-cost (cost of driving blood through the network) measured in watt is calculated as:

$$W = Q_{total}\Delta P_{total} \tag{39}$$

where Q_total is the flow through the system measured as the flow through the outer vessels (vessels of the highest generation), and ΔP is the pressure difference over the entire network.

However as mentioned, it is hypothesized that an increase in the total volume of the network as a result of vasodilatation also has a second cost for the system: An increased volume taken up by the stroma leaves less volume available for the parenchyma. The contents of this cost is further discussed in the discussion section. A linear function was used to describe this E-cost (also in watt):

$$f(V) = a * V \tag{40}$$

where V denotes the total volume of the network: The sum of volumes of all vessels. a is the slope of the function, which is a positive value. The exact value of the slope is found testing whether any values can give a U-shaped curve for the total cost, which is described in equation 41. Note that f(0) = 0 since it is assumed that there is no cost if there is no volume, and if the network volume increases infinitely, so will the E-cost.

The total cost function therefore consists of two terms:

$$W_{total} = f(V) + Q\Delta P \tag{41}$$

The simulations were generated to investigate whether a possible minimum in the above function could be found. Two sets of simulations were generated: Both with four generations of vessels, one with WI = 50% and one with WI = 6%. For each setting, three initial network configurations were investigated for a range of inlet pressures.

2.7 Sensitivity analysis

A local sensitivity analysis with use of statistical investigations was conducted on the following parameters: Initial oxygenation of tissues, γ_1, the intercept of the metabolism function (γ_2), G_ECEC, stimulus size, solubility, $V_{m_{slope}}$ and the dissipation regulation parameter. All but the two first and two last of these parameters were based on literature (see Table 1). However, all the parameters were modified on the basis of trial simulations in order to adapt them to the model. This is why they were chosen for analysis of sensitivity. Initial oxygenation level is an initial condition for the model. This parameter should ideally not have an influence on the final model result, as the model should be able to adapt away from it, and it was therefore chosen for sensitivity investigation.

The statistical analysis investigates how sensitive the above mentioned parameters are when comparing the radii of each vessel at the end of simulations. ANOVA tests were used to test for statistical differences between each vessel across three or more parameter levels. The resulting p-values were Bonferroni-corrected with regards to all performed ANOVAs. Capillaries were excluded from the analysis, since these cannot change radius. All simulations (10 simulations pr. parameter level) were run with WI = 50%, four generations and inlet pressure of 5333 Pa (40 mmHg). Parameters were generally increased or decreased by a factor of 10, or, in case of model crash or no significant differences, changed by +/- 10% or factors of 100. Normality distribution was checked with QQ plots, and possible directions of difference was tested with Tukey tests. The procedure of the analysis is illustrated

below.

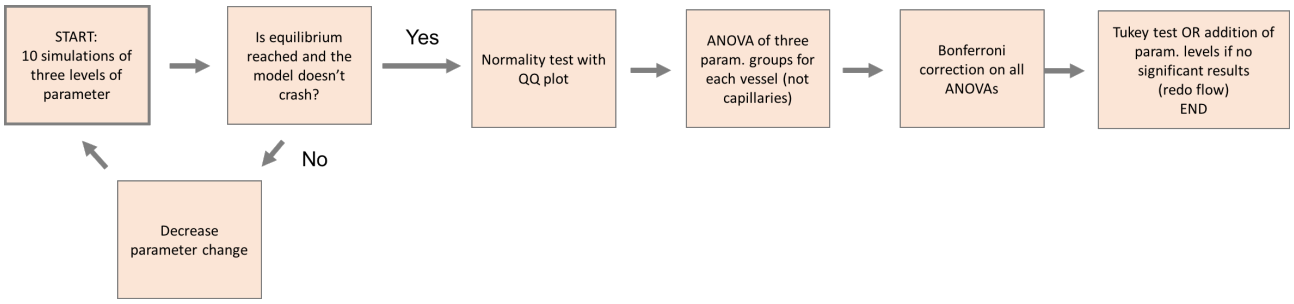

Figure 6: Pipeline for sensitivity analysis.

2.8 Parameter table

Parameter	Value	Unit	Description	R/E/A*	Literature
General parameters					
k1	$1.0 * 10^{-4}$	-	For vessel length	R	[28]
k2	0.5	-	For vessel length	R	[28]
c	3	-	For vessel radius	R	[28]
a (artery)	$6.0 * 10^{-6}$	-	For arterial radius	R	[28]
a (vein)	$1.5 * 10^{-5}$	-	For venous radius	R	[28]
μ	$4.0 * 10^{-3}$	Pa*s	Blood viscosity	R	[28]
capillary length	$1.0 * 10^{-4}$	m	Capillary base length	R/A	([28])
capillary radius	$5.0 * 10^{-6}$	m	Capillary base radius	R/A	([28])
time step	$1*10^{-2}$	s	Time step	-	-
P_{out}	2000	Pa	Outlet pressure	R	[7]
ρ	1060	kg/m^3	Blood density	R	[33]
Tissue oxygenation					
v	$1.0 * 10^{-3}$	m/s	Capillary blood velocity	R/A	[30]
[Hb]	150	kg/m^3	Hb concentration	R	[14]
Hüffner	$1.31 * 10^{-3}$	m^3/kg	Hüffner's constant	R	[14]
solubility	$2.1584 * 10^{-7}$	$m^3/(m^3 * Pa)$	Solubility of oxygen in tissue	R/(A)	[29]
PO_{2min}	2133	Pa	Minimum accepted tissue PO_2	R/A	[16]
PO_{2max}	2933	Pa	Maximum accepted tissue PO_2	R/A	[16]
γ_1	1.3	-	Diffusion regulation constant	E	-
pCapIn	13332	Pa	Inlet capillary PO_2	R	[9]
D	$2.1 * 10^{-9}$	m^2/s	Oxygen diffusion constant	R	[34]
WI_{slope}	7/432000	$m^3/(m^3 * s)$	Slope of metabolism function	E	[17]
$WI_{intercept}$	1/21600* γ_2	$m^3/(m^3 * s)$	Intercept of metabolism function	E	[17]
γ_2	$6 * 10^1$	-	WI regulation constant	E	-
pCr	66.66	Pa	Critical PO_2 in tissue	R	[29]
Flow regulation					
endothelialThickness	$0.75 * 10^{-6}$	m	Thickness of endothelium	R	[11]
$C_{m_{specific}}$	$1.0 * 10^{-2}$	F/m^2	Specific membrane capacitance	R	[11]
G_{ECEC}	$(1/(3 * 10^3))/(160 * 10^{-12}) * 2 * 10^{-5}$	$(A/V)/m^2$	EC-EC coupling conductance	R/A	[11]
Stimulus	$1.0 * 10^{-11}$	A	Metabolism stimulus	R/A	[11]
γ_3	$1.0 * 10^{-1}$	-	Modification of shear stress	E	-
tensionPotential_steep	200	-	Steepness of tension from Vm	E	-
variationRange	0.005	-	Radius change fixpoint	E	-

Table 1: Parameters used in the model with their used values, units, description, utilization and reference. ***R**: Parameters used exactly as retrieved in literature, **E**: Estimated parameters based on e.g. model trials, **A**: Adjusted parameters (often based on parameters from literature).

3 Results

The results generated from the simulations are chosen with two main purposes in mind: Evaluation of the model and answering the hypothesis of minimum cost for the MAP. Therefore, both the progression of variables and final states of the network are of interest, since both can shed light on the quality of the model, and the latter is necessary to answer the hypothesis. At last, the result of the sensitivity analysis is presented.

3.1 Simulations

As mentioned, a network of three generations was simulated for a range of P_{in} between 2666 Pa (20 mmHg) and 15332 Pa (115 mmHg) and WI = 50%. The results could be divided into three types of output: Two types where the model could not adapt to the given P_{in} (for very low and high inlet pressures, respectively), and one where the model adapts. First, a typical run from a successful adaptation will be presented, and afterwards the two "boundaries" for the model are described.

3.1.1 Successful adaptation

The figures 7 and 8 were characteristic for simulations in the P_{in} interval of about 4000-8000 Pa (30-60 mmHg). The results illustrate a simulation with four generations, a P_{in} of 5066 Pa (38 mmHg) and a work intensity of 50%.

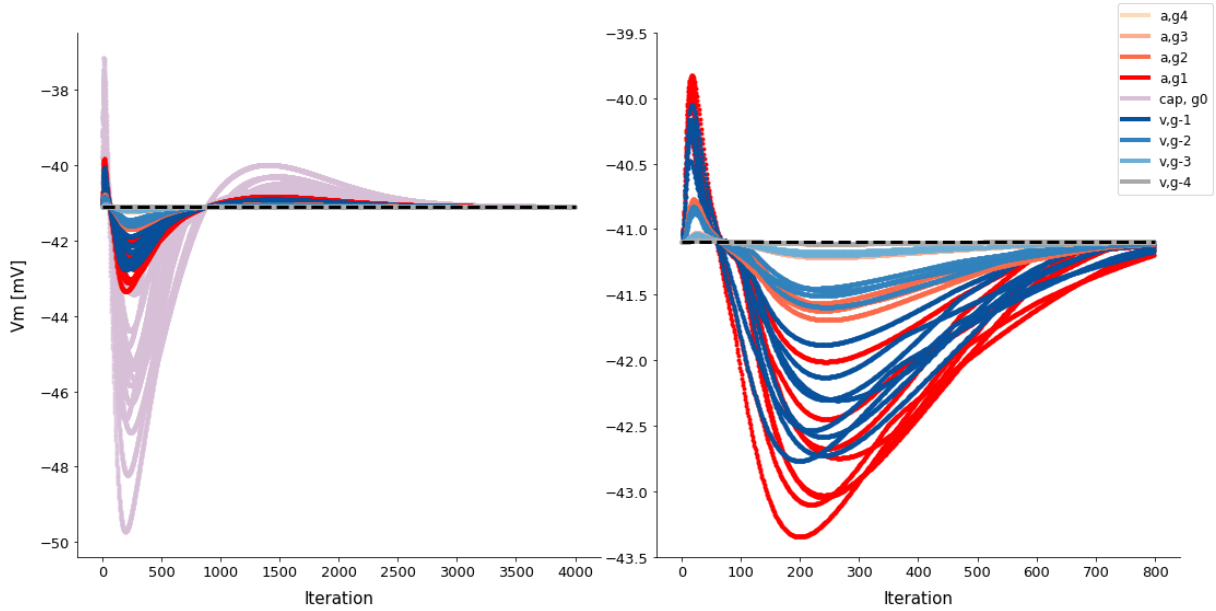

Figure 7: Development of membrane potentials (V_m) for a network of four generations, work intensity of 50% and inlet pressure of 5066 Pa (38 mmHg). Arterioles are shaded red, venules blue, and capillaries faded purple. Left: V_m for all vessels until the end of fluctuations. Right: V_m for all vessels except capillaries, showing only the first fluctuations.

Figure 7 (left) shows the simulation of membrane potentials in all vessels. Note that this plot is

shown to give an overview of all fluctuations, while the more exact developments of each vessels are shown in the plot to the right. Each line denotes a vessel, and the color denotes the generation. Capillaries are in faded purple, arterioles in increasingly dark red colors from the inlet and towards the capillary beds and venules in increasing dark blue colors from the outlet and towards the capillary beds. The black dashed line denotes $V_{m,rest}$ (-41.09 mV) [11], around which the potentials of vessels fluctuate. Note that although the actual simulation was longer, only the first 4000 iterations are illustrated, since all fluctuations around the resting membrane potential happen before iteration 4000. The figure to the right is a zoom on the fluctuations in all vessels apart from the capillaries, showing only the first 800 iterations. The graphs together show an initial depolarization (iteration 0-60), indicating a lack of oxygen which could be due to the initial oxygenation of the tissues. Afterwards, a hyperpolarization (iteration 60-900) indicates a lack of oxygen, which is consistent with a high level of metabolism (50%). At last before the steady state at the resting membrane potential, a few vessels above the $V_{m,rest}$ indicate an overload of oxygen in some capillaries. The capillary membrane potentials fluctuate in the between -37.12 mV and -50.37 mV, while the other vessels show decreasing amplitudes in fluctuation the higher the generation. Note that the arterial side of the network shows larger fluctuations than the venous side in the same generation. For example, generation 1 ranges between 39.82 mV and -43.35 mV, while generation -1 ranges between -40.06 mV and -42.77 mV.

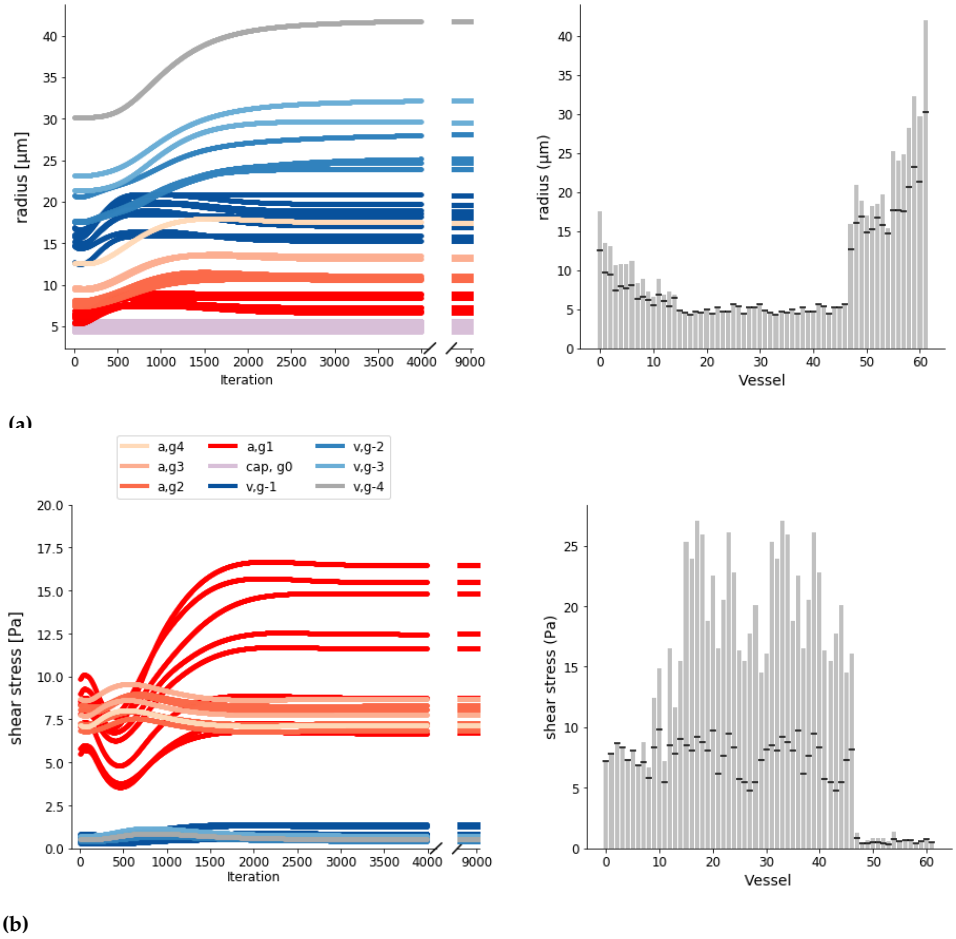

Figure 8: Development (left column) of radii (top row) and shear stress (bottom row) for network of four generations, work intensity of 50% and inlet pressure 5066 Pa (38 mmHg) (same simulation as Figure 7. Color codings are equal to Figure 7. Right column: Initial states (black lines) of radii and shear stress shown compared to final states (grey bars).

Figure 8 shows the progress of radii and shear stress (left column) for the same simulation as was reflected by the above membrane potentials. The same color coding applies as in Figure 7. The right column shows the change from initial values (black lines) and final values (grey bars) in radii (top) and shear stress (bottom). Note that shear stress in capillaries has not been illustrated since this stress has no effect on the model.

The course of the simulation of radii shows an initial slight decrease of radii in generation 1 (red) at the same time as the membrane potential depolarization, followed by a dilatation along with the depolarization. Most arterioles show an increase in radius until about iteration 1500, where some of them show a slight contraction. Most veins increase in radius until about iteration 3000 and then reach a constant level. A general steady sate is reached for most vessels after about 4000 iterations. For the shear stress, the same initial decrease and increase is seen within the first 500 iterations. After about 1500 iterations, the arterial shear stresses (generation 2, 3, 4) are back to the initial level, while the venular levels are back after about 3000 iterations, in correspondance with the radii. Note that

generations 1 (red) and -1 (dark blue) reach a new steady state, which is in accordance with the shear stress being modeled as non-influencing in these vessels.

The right column in Figure 8 shows the comparative radii of the initial network (black lines) and final steady state (grey bars). Capillaries do not change radius, as is reflected by the diagram. However, a symmetrical relative change in radii can be observed: A change in an arterial vessel is reflected by a similar relative change in the venous side of the network. For example, the ratio between the initial arterial g4 vessel and the final arterial g4 vessel is 1.3906, while the initial venous g-4 vessel and the final venous g-4 vessel is 1.3904. For the shear stresses, most vessels apart from capillaries and generation 1 and -1 end at the initial level.

Figure 9 (a) shows the change from initial blood pressures in the network nodes (black lines) and the final node pressures (grey bars) corresponding to the same simulation as described above. In both the beginning and end of simulation, there is gradual decrease in pressure across the network with most venous nodes having the lowest pressure. The right figure shows the spread of pressure drop ΔP for each vessel. While the pressure drop initially is largest at the inlet of the network and gradually decreases, at the end of the simulation the pressure drop is more evenly spread out in the network, until the venous side is reached (vessel 48) where very few changes happen.

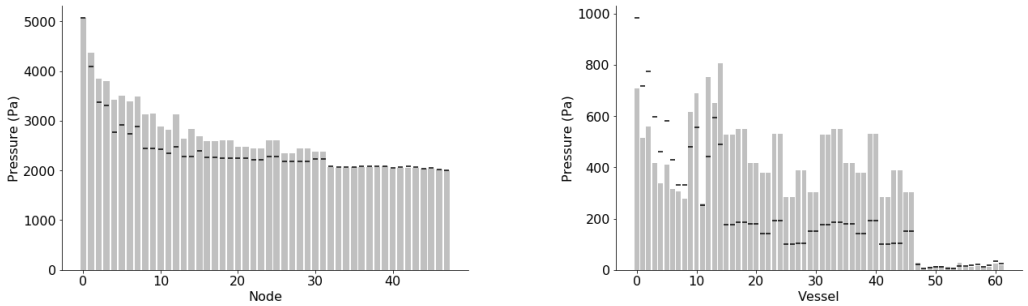

(a) **(b)**

Figure 9: Pressure development for a simulation with 4 generations, work intensity of 50% and inlet pressure 5066 Pa (38 mmHg). **a**: Pressure development from inlet node (node 0) to outlet node (node 47). **b**: Pressure drops per vessel. For both: Black lines indicate the pressure status before simulations start, grey bars the pressure status at equilibrium.

For the shown simulations, the hierarchy of vessel radii for increasing generation levels was generally kept. Turbulence did not occur in any runs.

3.1.2 Simulations of too high and low P_{in}

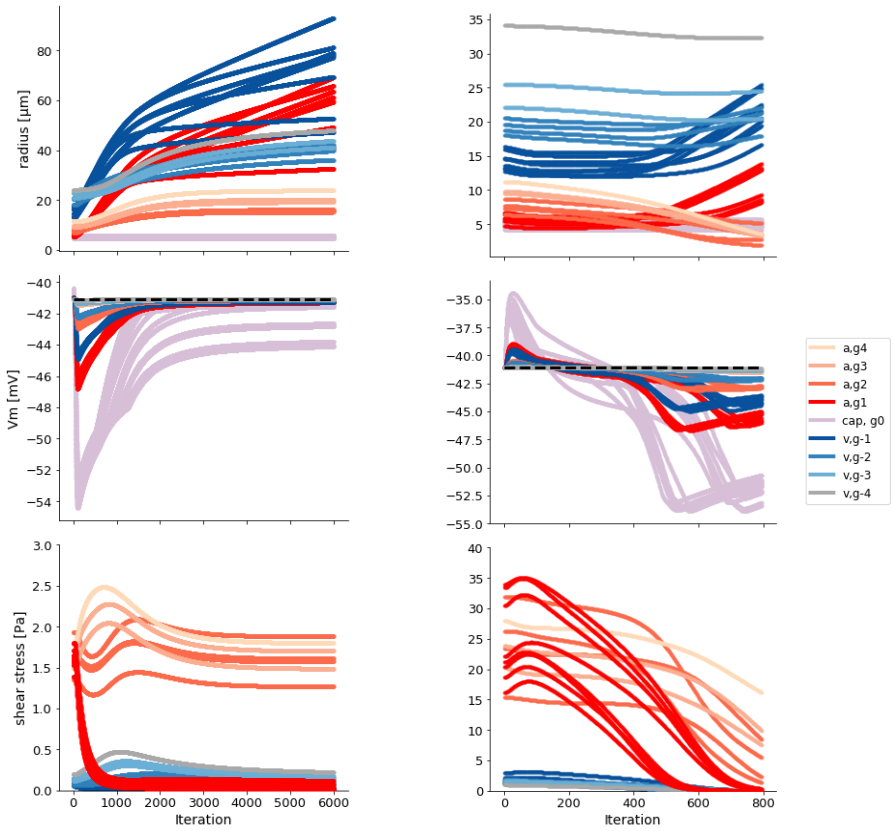

(a) P_{in} = 2666 Pa (20 mmHg)

(b) P_{in} = 12000 Pa (90 mmHg)

Figure 10: Simulations of radii, membrane potential and shear stress for a network with four generations, work intensity of 50% and inlet pressure of either 2666 Pa (20 mmHg) (**a**) or 12000 Pa (90 mmHg) (**b**). Note that capillary shear stress is not included.

Figure 10 show development of radii (top row), membrane potentials (middle row) and shear stress (bottom row) for simulations with the same conditions as the previously described simulations above, however with an inlet pressure of 2666 Pa (20 mmHg) (representative for simulations with inlet pressures under 400 Pa (30 mmHg)) and 12000 Pa (about 90 mmHg) (representative for inlet pressures of above 8000 Pa (60 mmHg)). In the left column (low pressure), the radii of the inner vessels (g1, g-1) exceed the radii of the vessels further from the capillaries and continue a constant increase, while the outer vessels get closer to a steady state phase. The membrane potentials of the capillaries indicate a constant lack of oxygen since there is a constant hyperpolarization of capillaries. For the shear stress, the outer arterioles and venules reestablish initial levels, while shear stress of generation 1 drops to almost zero. In the right column (high pressure), all radii change while initially keeping the order of the magnitude of radius between the generations, although there is an almost universal decrease of radii, in correspondence with the high inlet pressure containing perhaps too much oxygen for the tissues. After about 600 iterations, the inner vessels (generation 1, -1) start to increase again, seemingly in correspondence with a hyperpolarization of membrane potential, although the outer vessels keep

decreasing. At the same time, shear stress constantly decreases in all vessels. The model terminates after 797 iterations.

3.2 The cost of perfusion

In this section, results the costs of network perfusion is presented. First, work, pressure and network volume is evaluated without the evolutionary cost, and then the total cost (evolutionary and network cost) are viewed together.

3.2.1 Energy loss, network volume and pressure developments

The next graphs are generated based on simulations of several networks to observe relations and trends in PV-cost, network volume and pressure developments.

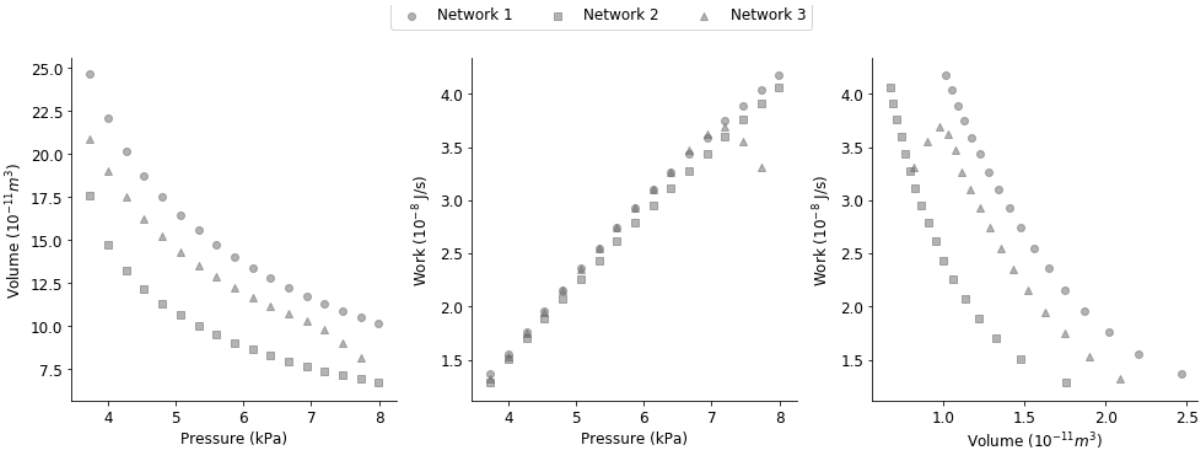

Figure 11: Development of total network volume, PV-cost and inlet pressure for three different initial network configurations (1, 2 and 3).

Figure 11 shows the relations between total network volume, PV-cost (in watt) (note that the E-cost is not included here) and P_{in} for three different networks simulated with P_{in} ranging from 3733-8000 Pa (28-60 mmHg), based on the boundary situations as described in the previous section. All networks were simulated with WI = 50% and four generations of vessels on each side of the capillary beds. Each symbol (square, triangle, circle) represents a network with the same initial vessel radii and lengths, so the inlet pressure is the only varying condition for the line of each symbol. The left figure illustrates the development of total network volume at different P_{in} levels. There is a gradual decline in network volume as the inlet pressure increases. The same goes for the middle figure, which shows that as P_{in} increases, the energy cost increases as well. At last, the figure to the right shows a decrease in energy costs as the volume of the networks increase.

3.2.2 Total costs and network volume

Figure 12 shows patterns for the sum of the two described costs: PV-cost and E-cost. The symbols represent three networks with each their initial network configuations, as described for Figure 11.

Note that the networks in the right column (a) and left column (b) are independent networks (therefore the names network A, B, C and 1, 2, 3). The left column (a) shows results for networks with WI = 6%. Here, simulations for inlet pressures between 2400 Pa (18 mmHg) and 3866 Pa (29 mmHg) were found to successful adaptatations. (A few simulations were however removed due to simulations similar to Figure 10) The left column, b, shows networks for WI = 50%.

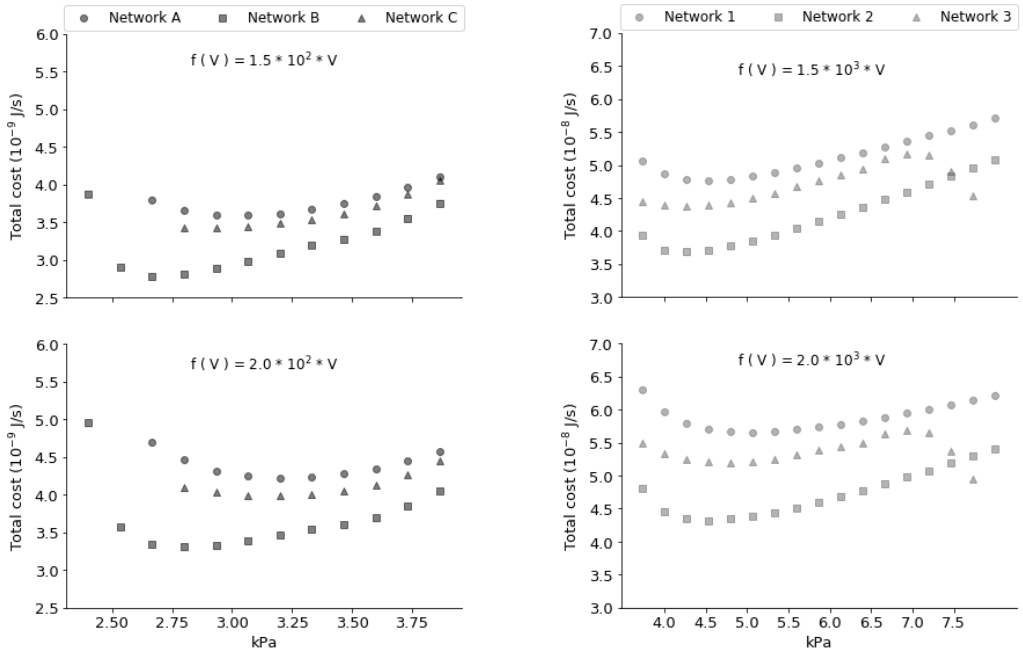

(a) Work intensity: 6%

(b) Work intensity: 50%

Figure 12: Total cost (PV-cost + E-cost) for six different networks (A, B, C, 1, 2 and 3). Network A, B and C (**a**) are simulated with a work intensity of 6% (dark grey), while network 1, 2 and 3 are simulated with a work intensity of 50% (light grey). The E-cost function for each simulation is shown in each graph.

As it can be seen from the function equations in the graphs, networks with WI = 50% had to be multiplied by an extra factor 10 for the evolutionary cost function to scale with the network perfusion costs.

Note that in both WI situations, a U-shape occurs and indicate a minimum cost. Also, in the upper row the evolutionary cost was created with a slope of 1.5 ($(N/(s*m^3)$), while the lower row shows evolutionary costs with a slope of 2.0 ($(N/(s*m^3)$). For the network in (a), the slope of 1.5 ($(N/(s*m^3)$) caused a minimum in the range 2.5-3.2 kPa (19-24 mmHg), while the slope of 2.0 cause a minimum between 2.6 kPa (20 mmHg) to 3.4 mmHg (25-26 mmHg). For the situation with WI:50%, the change in slope moved the minimum from about 4-5 kPa (30-37 mmHg) to 4.2-5.5 kPa (31-41 mmHg).

Network 3 in Figure 12b shows a dissimilar pattern from the two other network simulations at high inlet pressures. Upon visual inspection of the network, the vessels of this network only changed marginally, presumably allowing for a correct amount of oxygen reaching the tissues.

Finally, Figure 13 is shown for comparison of the volumes of the networks in Figure 12. Although only few simulations for each situation is included, a possible pattern seems to emerge: Networks with WI = 6% seem a little smaller in total network volume than networks with WI = 50%.

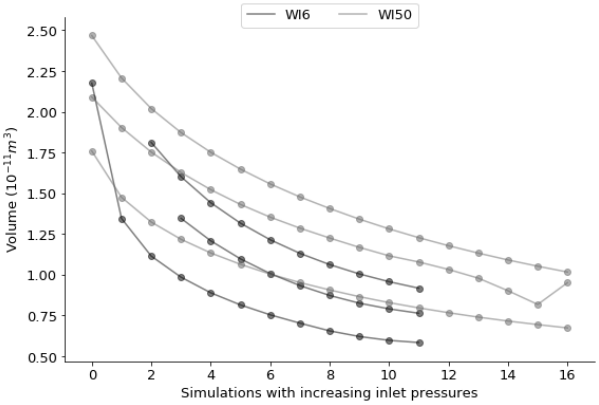

Figure 13: Total network volumes for simulations (same as in Figure 12) with increasing P_{in}. Dark lines indicate simulations with work intensity of 6%, light grey lines indicate simulations with work intensity of 50%.

3.3 Sensitivity analysis

Table 2[4] shows the parameters tested for sensitivity, the parameter values included for comparison and the number of vessels for each parameter test that were found significant after Bonferroni correction across all ANOVAs. All simulations were run with 11000 iterations. All data sets were confirmed by QQ plots [5] to be from a normal distribution.

For initial oxygenation of the tissues, no vessels were found to vary significantly from each other after Bonferroni correction. This was as expected and renders the initial oxygenation level without significance.

For γ_1, no equilibrium was reached when simulating with a change of +/- 10%. Both results was similar to the scenario in Figure 10a.

Both γ_2 (metabolism intercept) and solubility showed significant differences in final radii with changes of parameters of +/-10% ($p < 0.02$ and $p < 0.01$, respectively). Generally, higher solubility and metabolism lead to smaller vessels radii, and higher metabolism lead to larger vessel radii.

An increase ECEC coupling conductance by a factor 10 caused the membrane potentials to develop increasingly extreme values in correspondance with previously mentioned modification trials. However, gradual decrease had a smaller effect, although when comparing with the parameter multiplied by factors 10^{-3} and 10^{-4}, seven vessels were found to differ significantly.

Both the γ_3 (shear stress modification) and stimulus were found not to cause significant changes in more than 0 and 2 ($p < 0.03$) vessels, respectively (stimulus). However, stimulus size multiplied by a factor 100 caused the model to crash, and some sensitivity was therefore to be found. How-

[4]See Appendix B for Bonferroni correction within parameter groups.
[5]See example of QQ plot in Appendix C

Parameter	Parameter changes	Significantly differing vessels		
		Number of differing vessels	p_{adj} *for all vessels*	*Direction*
Initial oxygenation level	0, 7, 19, 31 mmHg	0	-	-
γ_1	$+/-10\%$	No equilibrium	-	-
G_{ECEC}	$*\,10^{-1}, 10^{-2}, 10^{-3}, 10^{-4}$	7	p <0.05	Lower G_{ECEC} cause lower radii
γ_2 (Met. intercept)	$+/-10\%$	27	p <0.02	Higher γ_2 cause higher radii
Solubility	$+/-10\%$	21	p <0.01	Higher solubility cause smaller radii
Stimulus	$*\,10^{1}, 10^{-1}, 10^{-2}$	2	p <0.03	Mixed directionality
variationRange	$*\,10^{1}, 10^{-1}, 10^{-2}$	13	p <0.01	$*\,10^{-2}$ cause smaller radii
γ_3 (SS)	$*10^{2}, 10^{1}, 10^{-1}$	0	-	-
Dissipation constant	$*\,10^{1}, 10^{-1}$	0	-	-
V_m *slope constant*	$*\,10^{1}, 10^{-1}$	0	-	-

Table 2: Overview of results from sensitivity analysis.

ever, variations in both factors caused a change in iterations before equilibrium, which was barely reached for some simulations. In general, an increase of the factors seemed to lead to longer time to equilibrium.

Lastly, for variationRange, an increase of a factor 100 caused the model terminate simulations. For the factors written in the table, it was found that a decrease of variationRange led to an increase iterations to equilibrium and 13 significantly differing vessels ($p < 0.01$). However for some simulations, equilibrium was barely reached. The ANOVAS were therefore performed under the assumption that the final state resembles equilibrium. For the dissipation constant and slope for the influence of V_m on SMC tension, no significant difference were found, but the number of iterations before equilibrium seemed to vary. These two were therefore not tested further.

Overall, the initial condition of oxygenation was found not to be sensitive, which was as expected. Parameters such as γ_1, G_{ECEC}, γ_2 and solubility were found to be very sensitive, since a change of a factor 10 or in some cases less could cause the model to crash or lead to meaningless results. Other constants, such as variationRange, stimulus size and γ_3 were not found to be quite as sensitive, but had an influence on the number of iterations before equilibrium. Due to computational load, significant differences for a wider range of values for these parameters were not investigated.

4 Discussion

The results for the two main project aims, 1) creating a model that can imitate biological adaptations and 2) whether MAP could be related to an energy cost minimum, are discussed in turn in this section. First, the simulation results and sensitivity analysis will be presented, followed by considerations about the U-shapes curves in Figure 12. Finally, considerations on the ontology of the E-cost, and overall considerations about all results are discussed.

4.1 Discussion of simulation results

The figures 7, 8, 9 showed the development of membrane potential, radii, shear stress and pressure change in the network for a simulation. In general, the development of radii seem possible to interpret from the effect of the membrane potentials and shear stress: The initial depolarization (Figure 7) cause the inner vessels to contract (Figure 8, followed by a large depolarization which causes all vessels to dilate. This increases the shear stress 8, and the vessels were found to continue dilatations as long as their respective shear stress was above its initial value, although the hyperpolarization did not last as long. Thereby, the vessels of higher generations dilated to somewhat maintain the hierarchy of vessel size, which was the point of the shear stress effect. From this point of view, the inclusion of shear stress effects seems successful. Equilibrium was reached after about 9000 iterations, the membrane potentials returned to the resting membrane potential, and the vessels whose shear stress have influence on dilatation and contraction ended up with a shear stress at the initial value. Looking at these influences, both the CVR and shear stress seem to have had the desired effect.

The final radius states were overall proportionally larger than the initial states. Poulsen et al [7], who also do computational modelling of microvascular network structure, also find a somewhat symmetrical (arteriolar vs. venous) pattern of internal final radii after simulations, which could support the acceptance of this result. However, Poulsen et al [7] investigate a more anatomically complex network structure where e.g. the vessel wall is also included. The results therefore cannot be completely parallelized with those of this project.

The final shear stress of the simulation (Figure 8) is between 5-10 Pa for the arterioles in which the SMC tension is affected by shear stress and below 1 for the venules. According to Ballerman [19], small arterioles typically have a shear stress of 6-8 Pa and small venules of 2-4 Pa. For the arterioles, this matches well with the result, although the result for the venules is a little lower than 2 Pa. The results are nevertheless in the correct scale. From Figure 8 it is also seen that the shear stress of generation 1 increases heavily without diminishing, as shear stress was removed from the tension function for this generation. In the plot showing the development of radii, this generation is also the main one to decrease in radius after the increase (following the membrane potential), and it therefore seems that the idea of letting the membrane potential govern this "final gateway" to the capillaries works.

The final states of node pressures 9 show that in general, the node pressures in the arterial and capillary part of the network increase during the simulation leading to a final larger drop when reaching the venules. At the same time, pressure drops across vessels happen more evenly throughout the

arterial and capillary vessels after simulations than when initiating the simulation. This does not correspond with the results of Poulsen et al [7], where the pressure decline happens symmetrically across the network. For the results of this project, the lack of a modelling the vessel wall could be influential here.

The fact that the hierarchy of vessel radii in increasing simulations was generally kept and the lack of turbulence can be interpreted as another validation of the model, since these were factors expected from the model.

Figure 7 showed that the amplitude of the capillary membrane potentials to be larger than the remaining vessels. This is in accordance with the capillaries as the site of stimulation and the combination of dissipation and conduction loss in the nodes. It therefore seems that a large amount of the current is lost at these branch points. This was also the case in the study from which several of the parameters in this model were adapted [11], which implies that these have been implemented beneficially. At the same time, the arterioles showed higher amplitudes than venoules, which corresponds with the virtual node potential as being a weighted mean of the vessels that branch from it: Since venoules have larger radii, they have a larger influence on the conducted potential from the capillary than the arterioles. Some studies and theories point to the arterioles as being the most important vessels for flow regulation [8], and some argue that the arterial wall is the only pathway for the conducted response [12]. However, there is also seems to be evidence for bidirectionality (both arteriolar and venous conduction) of the signal [8, 35], and the results and methodology of this model can therefore be viewed as reasonable.

The "boundary scenarios" in Figure 10 showed that two characterised extreme scenarios could occur. These scenarios were apparently dependent on the inlet pressure and thereby also the flow of blood and oxygen. It seems that in the first scenario (2667 Pa (20 mmHg)), the tissues do not receive enough oxygen, which is reflected by the constant hyperpolarized membrane potentials in the capillaries and constantly increasing raddii of the inner vessels (g1, g-1). Although it is likely that the oxygen delivery is simply too low, the lack of dilation from the upstreams generations cause concerns. In some closer investigations it was found that the radius change in some vessels was cancelled out by the tension input from V_m and SS – they simply opposed each other. If this is the case in the outer vessels, the inner vessels alone would be responsible for the adjustment of oxygen delivery. However, given the purpose of the shear stress to ensure a somewhat constant proportional relationship between the radii of the inner and outer vessels, it could be argued that in this case the shear stress is simply not adaptive enough. The diameters of the upstreams vessel do not allow enough blood to the inner vessels, which are therefore the main "fighters" for capillary blood flow. On the other hand, an inlet pressure as low as 20 mmHg for a WI = 50% may also simply be too low, and the system might possibly have stoppet dilating much earlier in vivo.

In the second extreme scenario (Figure 10b), it seems that the oxygen delivery is initially too large, causing the vessels to contract until the blood flow is large enough. However, this also causes a drop in shear stress in the higher generations, and from then the outer vessels keep contracting, while the inner vessels seem to react to the hyperpolarization that arises. In this case, it seems that the shear stress has too much effect – there is no end to its contracting effect on the outer vessels.

Overall, for the successful runs, the results can be explained in concordance with the methodology, and the developments are somewhat comparable to literature. On the other hand, the model cannot adapt to inlet pressures that are very high or very low. This could point to the necessity of adding criteria for model behavior in extreme cases. However, in both cases the effects of shear stress could be argued to be responsible for the outcome: In the first case the effect seems too not be ”adaptive” enough for its purpose, while in the second case, it seems to cause a positive feedback with the radii, which abrupts the model. In both cases, it could seem that once an effect of the shear stress is introduced, the outcome of this effect becomes somewhat predetermined and not sufficiently adaptive. A third interpretation could however also be that such extreme inlet pressures are simply unlikely in a biological system, and that other outcomes, such as vessel eruption, could occur.

4.2 Sensitivity analysis

The sensitivity analysis revealed that some parameters (G_{ECEC}, γ_1, γ_2 (metabolism intercept) and solubility) were found very sensitive in at least one direction, where the simulations could not be fulfilled. In most cases, this was to be expected from the parameter modifications. For example, the ECEC coupling conductance was modified with the aims of conducting as much current as possible from node to vessel without overwhelming the membrane potentials. However, some of the parameters are closely connected: γ_1, solubility and metabolism all have an influence on the consumption and delivery of oxygen in the tissues, and it is therefore possible that a different value combination could as well have let to reasonable results.

It might be considered whether differences between vessel size outcomes would be clearer if the noise on radii had not been as large as with a standard deviation of 10%. If the model were to be more finely tuned and the exact effect of parameters decided, it could be an idea to reduce this variance. Due to computational load of the problem, time and the amount of required tests, it was chosen not to perform this investigation in this project.

Overall, no parameters were found to be without effect on the simulation outcomes, and some even had very high sensitivity (e.g. γ_1), while some parameters (e.g. G_{ECEC}) had a somewhat wider range for possible values. Some parameters, such as the variation range and shear stress constant, were mainly found to influence the number of iterations before equilibrium, and these might therefore not have any effect on the final vessel radii states of the model.

4.3 Discussions of shear stress

As mentioned above, the effects of shear stress could be a central factor for issues with the outcome of the model simulations. The effect was one of the major challenges in making the model. In this section, the modeling of shear stress and its effects on vasodilatation and constriction is therefore discussed.

As previously described in the methods section, the effect of the SS on the tension of SMC is modelled as a combination of 1) the ratio of new SS compared to the original SS and 2) the magnitude of the shear stress (see equation 35). The first term causes the shear stress to fix towards an initial value.

The second term should ensure that larger shear stress would also lead to larger vessel diameter changes.

In the model, the shear stress should therefore be able to cause both dilatation and contraction. Generally shear stress is described as causing increases in vessel diameter [20, 19], and the model simulation with a constant contraction (Figure 10b) could therefore be unrealistic compared to a real biological system. However, some studies show a positive correlation between the size of shear stress and diameter of vessels [20], and it could therefore by hypothesized that if the shear stress decreases, the vessel diameter could also decrease.

The feature of a fix point (set as the initial shear stress) as determining for changes in the SMC tension was chosen in order to ensure some stability in the model. Furthermore, since this fixpoint is individual for each vessel and set as the initial shear stress of that particular vessel, there is no uniform setpoint in the network. This is in line with the studies by Pries et al. [36]: In this paper, Pries et al. argue against a uniform fixpoint based on experiments. They present the hypothesis that the vascular systems make structural adaptations to maintain a local wall shear stress, which is fixed around a value which is dependent on local transmural pressure [36]. Although transmural pressure is not included in the present model, the idea of a local fixpoint is reflected in the model. As an opposite viewpoint, Jacobsen et al. [37] describe studies that have found that a stabile adaptation is only reached with an initial mean value of shear stress of the system compared to a local initial shear stress. However, as Jacobsen et al. [37] also point out, there is no known way for the network to sense a mean wall stress in the network. The local fixpoint of the present model therefore seems like reasonable solution to the stability problem.

From the sensitivity analysis, it can be questioned whether the effect of the second term of the above mentioned equation is too pre-determined. The analysis found that a parameter modification of factor 10^{-2} eliminated the effects of the shear stress, causing extreme dilatations of the inner. However, the rest of the tested variations of γ_3 (the SS constant) did not have any influence on the vessel radii. It was expected that too large an influence from shear stress would dominate the effects of the membrane potentials – this apparently was not the case. Instead, it seems that a larger shear stress effect simply influenced the number of iterations to equilibrium. This suggests that the shear stress effects of the model may be too predetermined, since a variety of factors lead to the same final outcome. This could diminish the credibility of the results, if this causes e.g. a “fixed” dilatation, no matter the P_{in}. This is in line with the interpretation of the ”extreme inlet pressure” simulations (Figure 10), where the shear stress did not seem to adapt advantageously.

Overall, the basic principles of the shear stress effect in the model seems to be in accordance with some theories and models of shear stress. However, based on the sensitivity analysis and results from the simulations, it seems that in extreme situations, the shear stress does not necessarily act beneficially. The effects of the shear stress may possibly be somewhat pre-determined, which could lead to doubts about whether the final network radii at the end of simulations can actually simulate a real biological system.

4.4 Cost curves

In this section it is discussed whether the hypothesized "minimum" of total energy cost (PV-cost + E-cost) could be found.

Figure 11 showed that for the three simulations with work intensity of 50%, volume decreased with higher blood pressure, energy cost increased, and energy cost decreased with increased volume. This was to be expected: A larger pressure drop across the network implies a larger energy cost, and the larger the pressure, the less it is necessary for the vessels to dilate to increase the blood flow. Based on this, it was possible to make further discussions about the total cost of energy loss and evolutionary cost.

Figure 12 a and b showed that is was possible to generate a U-shaped total cost curve for simulations with a work intensity of 6% (setup WI6) as well as 50% (setup WI50). This means that possible energy cost minima were found in both cases. However, it was necessary to multiply the WI50 network volume, which is the input for the E-cost function, by 10 compared to the WI6 network to scale the cost with the PV-cost. This is presumably due to a higher energy cost of the blood flow in WI50 caused by the higher inlet pressures required for reasonable simulations (unreasonable simulations would e.g. be similar to simulations in Figure 10). To compare the results of two similar inlet pressure ranges for the two simulations, it would be fortunate if the model could be expanded to handle wider inlet pressure ranges than currently.

Minimum cost intervals could be found for both situations, but the interval was lower for WI6 (2.5-3.4 kPa) than WI50 (4-5.5 kPa). It therefore seems that an increased metabolism requires a larger pressure, which could be expected. Interestingly, variations in the slope of the E-cost function was able to move the inlet pressure range; a larger slope (e.g. 2 compared to 1.5) would in both WI situations increase the interval of P_{in} in which the cost minima could be found. This could reflect the effects of a vasodilatation: When more space is taken up by the network, this will make the E-cost increase (given that the MAP is the same). It also suggests that the slope (the cost per volume level) of the E-cost function could be determining for the magnitude MAP i mammals. Therefore, if mammals pay the same E-cost of network size and have similar anatomical structures in their microvasculature, this could lead to a common optimal MAP.

In this model, vessels are simulated without vessel walls. In the studies of network adaptation by Poulsen et al [7] and a metaanalysis by Pries and Secomb [38], it was found that wall thickness increases when transmural pressure increases. This suggests that the WI50 setup, where blood pressure is generally higher than in WI6, might theoretically have thicker vessel walls. This would increase the total network volume for these in the WI50 simulations, which would result in an even higher cost. However, wall thickness is closely related to circumferential wall stress, and studies suggest that signals from both shear stress, metabolic status and circumferential wall stress is necessary to create a well functioning model of microvascular networks [38]. If the model of this project was to be used for further investigations, it would be relevant to include the effects of circumferential wall stress and vessel walls.

If the WI50 setup would have increased wall thickness, the cost of total network volumes would indicate that WI6 is a more favourable situation. Also, it can be assumed that mammals are most of

the time in a state of rest, and it would therefore be favourable for the system to spare energy at this condition. WI6 should then be the optimal situation to which the E-cost should adapt, while the WI50 can be regarded as a transient state. Here it is also interesting to note that the WI50 network volumes were generally larger than WI6 (see Figure 13). This suggests that the WI6 has room to dilate in case of a sudden increase of tissue metabolism. This could be seen as a possible vascular flow reserve, which is the ability of sudden dilatation to increase tissue perfusion [28]. However, no statistical analysis for the differences in volume was carried out, and the observation therefore remains a hypothesis for possible further investigation.

If the WI6 situation is the more favourable, the model suggests an optimal inlet pressure at 2.5-3.4 kPa (19-26 mmHg), which is not consistent with values found in the literature: In this model, the network is simulated for four generations. According to the studies based on pressure in cat skeletal muscle, arterioles with the diameters of the fourth (24 μm) and fifth (30μm) generation should have a pressure of 70-75 mmHg [39]. However, given the already described issues of high and low pressures in the model, the accepted interval of oxygenation in the tissues and the apparent sensitivity of many of the model parameters, it seems likely that this minimum may well be the result of parameter combinations. The finding of a possible minimum cost interval is still regarded as the main result.

As a final comment on Network 3 in Figure 12b: This network had a lower total cost for very high inlet pressures than for lower, and the inspection showed that only small changes happened in this network, and the network size was probably suitable for the high inlet pressure and metabolism. However, simulations such as illustrated in Figure 10 showed that in very high or low pressures, alternative simulation outcomes could occur. Since the deviations in the Network 3 line occur in for high P_{in} values, the result is for now considered as a coindicidence from the possible large variations in network radii and lengths.

4.5 Integration of results

The question remains of how the interpretation simulation results affect the interpretation of the generated U-curves and energy cost minima. Is the model sufficiently well-functioning to allow us to trust the interpretations of total energy costs?

On the one hand, many elements indicate that the model works well: A wide range of simulations within certain P_{in} values seemed successful and many results (such as shear stress values, hierarchy of vessel radius, lack of turbulence, the spread of CVRs and an unsensitive initial condition for simulations) seemed in accordance with values and theories from literature. On the other hand, doubts can be raised about the credibility of the effects of the shear stress, the final state of blood pressure drops and some sensitive parameters. The U-shaped cost curves showed a range of P_{in} values as possible pressure minima, and based on this result, the model seems to confirm the hypothesis of MAP being related to a cost optimum weighted between the PV-cost and the E-cost. However, given the doubts about the model and its simulations, one could also argue that the model *seems* to confirm that such a cost optimum might exist wihtout actually confirming the theory.

4.6 Evolutionary cost

In this project, it is assumed that when the total volume of the distribution network (the sum of volumes of all vessels) increases because of vasodilatation, this leaves less space for the parenchyma. This means that even though a larger network may result in a smaller PV-cost, a price is paid for lack of space for the parenchyma. This price has been described as the E-cost. But what could be the ontology of this cost? In this sections, some thoughts on this cost, its content and its biological ground are presented.

The following can be thought of as possible set point values for the E-cost: First of all, the E-cost is assumed to depend on the total volume of the network (V). Therefore, if there is no network (volume = 0), then there must be no cost: cost(V=0) = 0. Oppositely, if the volume of the network grows infinitely, then there must be an infinite cost: cost(V=infinity) = infinity. In the project, these two considerations made way for the linear E-cost function: f(V) = a*V. However, neither of these extreme set points seem realistic. So what is the development of the cost between these two? Since some kind of blood flow is necessary, a minimum volume of a network must be necessary. This could for example be based on the size of the erythrocytes carrying oxygen, which would require a certain vessel size. However, it is still possible that this comes with a minor cost. Another question is the manner of increasing cost with increasing volume: Does the cost grow linearly, exponentially or in third manner? In this project, a linear manner has been tested, but investigation of other possible developments would be interesting to investigate in the future.

A second question is: *Why* would there be this cost? How can it be related to metabolism? One idea is that when the network volume increases, the parenchyma (in this project, the skeletal muscle tissue) would have to optimize its own functionality. This could be costly if the same level of activity was to be performed. Another idea is that if each vessel grows in volume and takes up more space, the distance between the vessels will increase to make room for the tissues that they supply. Here the cylinder-model, where one capillary supplies one tissue slab, is assumed. This could in the end increase the size of the entire organism, but it could also affect the angles with which the vessels branch. Optimal branching angles and the minimal amount of work required to make blood flow past angles have been investigated in previous studies [40]. However, it could be possible that larger general vessel volumes could have an influence on branching angles. If this is the case, the E-cost is closely connected to the PV-cost.

Alternatively, a high metabolic rate could be related to higher capillary density. This is for example the case in flight muscles in migrating birds [41]. This could both cause a larger resistance in the network, more branching and perhaps an increased total network volume - which would fit with the fact that birds have higher MAP than mammals [3]. Based on these thoughts, it could be interesting to look at anatomical differences in vessel branching and structure. Could there be something non-universal in the structural relations between vessels and parenchyma cross species?

The considerations about capillary density also be related to the assumptions of the present model: In the model, capillary density is not included as a variable, and the tissue slabs supplied by a capillary are denoted a constant volume no matter the work intensity. It is assumed that one capillary supplies one tissue slab independently of other capillaries. However, this could be a bias in the esti-

mation of network volume and the energy used to supply the tissue.

No matter what the cost consists of, if it has something to do with branching angles, network structure or the like, one thing seems apparent: The PV-cost and the E-cost cannot exist independently. However at this point, we cannot tell how they are intertwined.

Finally: Can it not be considered obvious that an increasing PV-cost, which should decrease with increasing network volume, and an increasing E-cost, which should increase with increasing network volume, *must* reveal some minimum energy cost when they are added together? This might especially be the case in this project, where the E-cost is simply investigated as "which function can make it work". Perhaps it is obvious. But although this outcome may *seem* obvious, it is still relevant to try to falsify this assumption. The vascular network could possibly have developed or adapted in an arbitrary number of ways. Whether a minimum can be found in the present shape of the network is in this project regarded as an interesting topic - and if no minimum could be found, how could we explain that? Such a result could have led to further interesting hypotheses of the mammalian MAP.

5 Conclusion

It was to some degree possible to create a self-regulating model of a microvascular system by integrating two different regulatory mechanisms: Conducted vascular responses and wall shear stress. The model was on many aspects found to simulate reasonable results compared to biological considerations in literature. However, it was found that for a given metabolism level, the model could only adapt appropriately for a certain range of network inlet blood pressures. The modeled effects of shear stress was also considered to be too pre-determined and the precision of the simulated network configurations was therefore questioned. This was supported by the findings of sensitive model parameters. To increase the certainty of the model results, further investigations of modeling of shear stress effects are particularly recommended.

When an energy cost was calculated as the sum of the energy loss from driving blood through the simulated microvascular network and a linearly increasing energy cost of increasing network volume (evolutionary cost), minimum values of energy loss were found. These minima depended on the metabolism rate in the simulated tissues and the slope of the evolutionary cost function. However, the pressures did not correspond to expected blood pressures at the simulated vessel levels, although this could be due to the model parameter settings. In consequence, the results indicate that the mammal MAP could in fact be the result of an energy cost optimum, although an optimum of 100 mmHg was not found. Yet given the uncertainly of the precision of the model, it is mainly suggested that the hypothesis should not be rejected and further studies of the matter are encouraged. In such further studies, it is suggested to include capillary density, a vascular wall and effects of circumferential wall stress as model elements.

6 Perspectives and future investigations

As written in the report, several model expansions are suggested to investigate the relation between mammal MAP and tissue perfusion: First of all, a thorough investigation of possible shear stress mechanisms is encouraged. Such investigations could include comparisons between different models for the effects of shear stress on radius change or literature reviews of findings on the shear stress mechanism. Second of all, a vessel wall, which is found in many methodologically similar studies (e.g. Poulsen et al. [7]) and circumferential wall stress seem to be relevant for developing models that can simulate realistic biological structures.

Another relevant element could be anatomical investigations of differences in the microvascular structure across animal species - e.g. mammals, bird and amphibians. This could for example include evaluations of capillary density and branching angles in vessels. Such investigations could contribute to the understanding of the evolutionary cost of vascular network volume and the differences between MAP in e.g. mammals and birds.

References

[1] C. VanPutte, J. Regan, and A. Russo, *Seeley's Essentials of Anatomy and Physiology*. McGraw-Hill Education, 9 ed., 2016.

[2] R. S. Seymour and A. J. Blaylock, "The principle of laplace and scaling of ventricular wall stress and blood pressure in mammals and birds," *Physiological and Biochemical Zoology*, vol. 73, no. 4, pp. 389–405, 2000.

[3] R. S. Seymour, C. L. Bennett-Stamper, S. D. Johnston, D. R. Carrier, and G. C. Grigg, "Evidence for endothermic ancestors of crocodiles at the stem of archosaur evolution," *Physiological and Biochemical Zoology*, vol. 77, no. 6, pp. 1051–1067, 2004.

[4] C. B. Poulsen, T. Wang, K. Assersen, N. K. Iversen, and M. Damkjær, "Does mean arterial blood pressure scale with body mass in mammals? – effects of measurement of blood pressure," *Acta Physiologica*, vol. 222, no. 4, 2018.

[5] C. R. White and R. S. Seymour, "The role of gravity in the evolution of mammalian blood pressure," *Evolution*, vol. 68, no. 3, pp. 901–908, 2013.

[6] P. H. Sandal, M. Damgaard, and N. H. Secher, "Comments on the Review 'Does mean arterial blood pressure scale with body mass in mammals? Effect of measurement of blood pressure' Acta Physiol (Oxf)," *Acta Physiologica*, vol. 228, no. 1, pp. 2–3, 2020.

[7] C. B. Poulsen, M. Damkjær, B. O. Hald, T. Wang, N. H. Holstein-Rathlou, and J. C. B. Jacobsen, "Vascular flow reserve as a link between long-term blood pressure level and physical performance capacity in mammals," *Physiological Reports*, vol. 4, no. 11, pp. 1–21, 2016.

[8] T. W. Secomb, "Theoretical models for regulation of blood flow," *Microcirculation*, vol. 15, no. 8, pp. 765–775, 2008.

[9] J. G. Betts, K. A. Young, J. A. Wise, E. Johnson, B. Poe, D. H. Kruse, O. Korol, J. E. Johnson, M. Womble, and P. DeSaix, *Anatomy & Physiology*. Houston, Texas: OpenStax, 2013.

[10] J. E. Fletcher, "Mathematical Modeling of the Microcirculation," *MATHEMATICAL BIOSCIENCES*, vol. 38, pp. 159–202, 1977.

[11] B. O. Hald, "A generative modeling approach to connectivity-Electrical conduction in vascular networks," *Journal of Theoretical Biology*, vol. 399, pp. 1–12, 2016.

[12] D. G. Welsh, C. H. T. Tran, B. O. Hald, and M. Sancho, "The Conducted Vasomotor Response: Function, Biophysical Basis, and Pharmacological Control," *Annual Review of Pharmacology and Toxicology*, vol. 58, no. 1, pp. 391–410, 2018.

[13] D. Lu and G. S. Kassab, "Role of shear stress and stretch in vascular mechanobiology," *Journal of the Royal Society Interface*, vol. 8, no. 63, pp. 1379–1385, 2011.

[14] J. O. Dunn, M. G. Mythen, and M. P. Grocott, "Physiology of oxygen transport," *BJA Education*, vol. 16, no. 10, pp. 341–348, 2016.

[15] A. Krogh, "The number and distribution of capillaries in muscles with calculations of the oxygen pressure head necessary for supplying the tissue.," *Journal of Physiology*, vol. 52, pp. 409–15, 1919.

[16] E. Ortiz-Prado, J. F. Dunn, J. Vasconez, D. Castillo, and G. Viscor, "Partial pressure of oxygen in the human body: a general review.," *American journal of blood research*, vol. 9, no. 1, pp. 1–14, 2019.

[17] J. B. West and A. Luks, *West's Respiratory Physiology: The Essentials*. Lippincott Williams and Wilkins, 10 ed., 2015.

[18] R. Pittman, "The Respiratory System and Oxygen Transport," in *Regulation of Tissue Oxygenation*, ch. Chapter 3:, Morgan & Claypool Life Sciences, 2011.

[19] B. J. Ballermann, A. Dardik, E. Eng, and A. Liu, "Shear stress and the endothelium," *Kidney International, Supplement*, vol. 54, no. 67, pp. 100–108, 1998.

[20] A. Koller, D. Sun, and G. Kaley, "Role of shear stress and endothelial prostaglandins in flow- and viscosity-induced dilation of arterioles in vitro," *Circulation Research*, vol. 72, no. 6, pp. 1276–1284, 1993.

[21] L. J. Jensen and N. H. Holstein-Rathlou, "The vascular conducted response in cerebral blood flow regulation," *Journal of Cerebral Blood Flow and Metabolism*, vol. 33, no. 5, pp. 649–656, 2013.

[22] V. J. Schmidt, S. E. Wölfle, M. Boettcher, and C. de Wit, "Gap junctions synchronize vascular tone within the microcirculation," *Pharmacological Reports*, vol. 60, no. 1, pp. 68–74, 2008.

[23] M. Riemann, A. Rai, A. T. Ngo, M. H. Dziegiel, N. H. Holstein-Rathlou, and C. Torp-Pedersen, "Oxygen-dependent vasomotor responses are conducted upstream in the mouse cremaster microcirculation," *Journal of Vascular Research*, vol. 48, no. 1, pp. 79–89, 2010.

[24] M. Brorsen and T. Larsen, *Lærebog i hydraulik*. Aalborg: Aalborg Universitetsforlag, 2 ed., 2014.

[25] N. Westerhof, N. Stergiopulos, and M. I. Noble, *Snapshots of Hemodynamics. An Aid for Clinical Research and Graduate Education*. Springer, 2 ed., 2010.

[26] K. Schmidt, "eNote 8: Kvadratiske matricer," in *Matematik 1: eNoter*, 2015.

[27] K. Schmidt, "eNote 6: Lineære ligningssystemer," in *Matematik 1: eNoter*, 2015.

[28] J. C. B. Jacobsen, M. S. Hornbech, and N. H. Holstein-Rathlou, "Significance of microvascular remodelling for the vascular flow reserve in hypertension," *Interface Focus*, vol. 1, no. 1, pp. 117–131, 2011.

[29] M. L. Ellsworth, A. S. Popel, and R. N. Pittman, "Assessment and impact of heterogeneities of convective oxygen transport parameters in capillaries of striated muscle: Experimental and theoretical," *Microvascular Research*, vol. 35, no. 3, pp. 341–362, 1988.

[30] K. P. Ivanov, M. K. Kalinina, and Y. I. Levkovich, "Blood flow velocity in capillaries of brain and muscles and its physiological significance," *Microvascular Research*, vol. 22, no. 2, pp. 143–155, 1981.

[31] J. W. Severinghaus, "Simple, accurate equations for human blood O2 dissociation computations," *Journal of Applied Physiology Respiratory Environmental and Exercise Physiology*, vol. 46, no. 3, pp. 599–602, 1979.

[32] G. Grist, "Oxygen Pressure Field Theory: A detailed description of vital gas exchange, at the capillary level for perfusionists," *Progress in Pediatric Cardiology*, vol. 24, no. 2, pp. 89–99, 2008.

[33] D. J. Vitello, R. M. Ripper, M. R. Fettiplace, G. L. Weinberg, and J. M. Vitello, "Blood Density Is Nearly Equal to Water Density: A Validation Study of the Gravimetric Method of Measuring Intraoperative Blood Loss," *Journal of Veterinary Medicine*, 2015.

[34] D. Hershey and T. Karhan, "Diffusion Coefficients for Oxygen Transport in Whole Blood," *AlChE Journal*, vol. 14, no. 6, pp. 969–972, 1968.

[35] K. Tyml, H. Song, P. Munoz, and Y. Ouellette, "Evidence for K+ channels involvement in capillary sensing and for bidirectionality in capillary communication," *Microvascular Research*, vol. 53, no. 3, pp. 245–253, 1997.

[36] A. R. Pries, T. W. Secomb, and P. Gaehtgens, "Design Principles of Vascular Beds," *Circulation Research*, vol. 77, no. 5, pp. 1017–1023, 1995.

[37] J. C. B. Jacobsen, M. S. Hornbech, and N. H. Holstein-Rathlou, "A tissue in the tissue: Models of microvascular plasticity," *European Journal of Pharmaceutical Sciences*, vol. 36, no. 1, pp. 51–61, 2008.

[38] A. R. Pries and T. W. Secomb, "Control of blood vessel structure: Insights from theoretical models," *American Journal of Physiology - Heart and Circulatory Physiology*, vol. 288, no. 3 57-3, pp. 1010–1015, 2005.

[39] K. Fronek and B. W. Zweifach, "Microvascular Pressure Distribution in Skeletal Muscle and the Effect of Vasodilation," *American Journal of Physiology*, vol. 228, no. 3, pp. 791–796, 1975.

[40] C. D. Murray, "The Physiological Principle of Minimum Work Applied to the Angle of Branching of Arteries," *The Journal of General Physiology*, vol. 9, pp. 835–841, 1926.

[41] P. J. Butler, "The physiological basis of bird flight," *Philosophical Transactions of the Royal Society B: Biological Sciences*, vol. 371, no. 1704, 2016.

Appendix

6.1 Appendix A: Energy cost (PV-cost)

In a pipe, the energy cost is proportional with the energy drop between two cross-sectional areas [24]:

$$W_{heat} = \gamma Q \Delta H_{AB} \tag{42}$$

where γ is the specific gravity (kg/m^2s^2), Q (m^2/s) is the flow in the system and ΔH is the energy loss between cross-section A and B in meters. Laminar flow is assumed. Given the known pressure difference in the system, ΔP, it can be argued that ΔP encapsules the energy loss, which originates from resistance of friction and the divergence of the vessels in the system [24]. Also, since $[\gamma] * [H_{AB}] = kg/m^2s^2 * m = kg/ms^2 = Pa$ [24], that leaves the energy loss in the pipe:

$$W_{heat} = Q \Delta P \tag{43}$$

where W_{heat} is the energy loss in watt, Q is the blood flow in the given vessel and ΔP is the pressure difference between two cross-sectional areas of the pipe.

6.2 Appendix B: Full statistics results

Parameter	Values	Significant ANOVAs	Bonf. per parameter	Bonf. across all parameters	Notes (visual inspection, Tukey tests)
Initial oxygenation	0, 7, 19,31	2	None	None	As expected
gamma_1	* 0,9; 1,1	-	-	-	Not applicable to model
G_ECEC	* 1e-1, 1e-2, 1e-3, 1e-4, (1e1	25	15 (p < 0.04)	7 (p < 0.05)	The lower the G_ECEC, the smaller radii
gamma_2 (Met.int.)	* 0,9; 1,1	30	30 (p < 0.02)	27 (p < 0.02)	The lower the intercept, the smaller radii
Solubility	* 0,9; 1,1	30	25 (p < 0.03)	21 (p < 0.01)	Higher solubility, lower radii
Stimulus	* 1e1, 1e-1, 1e-2	12	5 (p < 0.03)	2 (p < 0.03)	Variation in results
variationRange	* 1e1, 1e-1, 1e-2	22	15 (p < 0.04)	13 (p < 0.01)	Equilibrium barely reached, 1e-2 cause smaller radii
gamma_3 (SS)	* 1e2, 1e1, 1e-1	6	1 (p < 0.05)	None	Time to equilibrium changes
Dissipation constant	* 1e1, 1e-1	5	1 (p < 0.05)	None	Time to equilibrium changes
Slope for tension_Vm	* 1e1, 1e-1	4	None	None	Time to equilibrium changes

Figure 14: All statistics results.

6.3 Appendix C: Example of QQ plot evaluation

The QQ plot below is based on a result for the parameter V_m slope decreased by a factor 10. The dots follow the diagonal line, indicating a normal distribution of data.

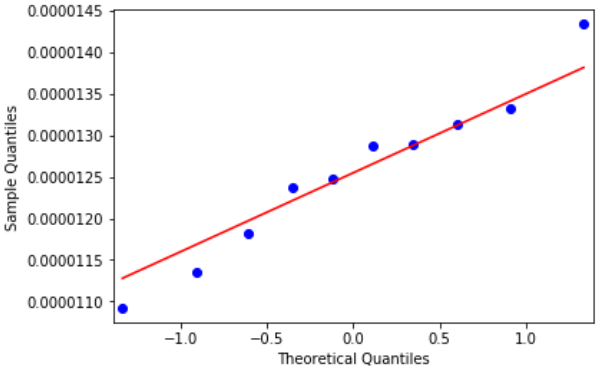

Figure 15: Example of QQ plot visualization based on the parameter V_m slope constant decreased by a factor 10.

6.4 Appendix D: Python and R code

The following scripts have been handed in as separate files:
main.py: Main simulation loop
functions.py: All functions used in the main simulation loop
statistics.py: File loadings and computations for statistics
Ushape.py: Script for generation of U-shaped curves (total cost)
PO2SO2curve.R: Fit for oxygen saturation curve.
plotExampleVm.py: Example of membrane potential plot